

Article

Prospects for Heavy Neutral SUSY HIGGS Scalars in the hMSSM and Natural SUSY at LHC Upgrades

Howard Baer^{1,2,*} , Vernon Barger², Xerxes Tata³ and Kairui Zhang²¹ Homer L. Dodge Department of Physics and Astronomy, University of Oklahoma, Norman, OK 73019, USA² Department of Physics, University of Wisconsin, Madison, WI 53706, USA³ Department of Physics and Astronomy, University of Hawaii, Honolulu, HI 53706, USA

* Correspondence: baer@ou.edu

Abstract: We examine production and decay of heavy neutral SUSY Higgs bosons $pp \rightarrow H, A \rightarrow \tau\bar{\tau}$ within the hMSSM and compare against a perhaps more plausible natural supersymmetry scenario dubbed $m_h^{125}(\text{nat})$ which allows for a natural explanation for $m_{\text{weak}} \simeq m_{W,Z,h} \sim 100$ GeV while maintaining $m_h \simeq 125$ GeV. We evaluate signal against various Standard Model backgrounds from $\gamma, Z \rightarrow \tau\bar{\tau}, t\bar{t}$ and vector boson pair production VV . We combine the transverse mass method for back-to-back (BtB) taus along with the ditau mass peak $m_{\tau\tau}$ method for acollinear taus as our signal channels. This technique ultimately gives a boost to the signal significance over the standard technique of using just the BtB signal channel. We evaluate both the 95% CL exclusion and 5σ discovery reach in the m_A vs. $\tan\beta$ plane for present LHC with 139 fb^{-1} , Run 3 with 300 fb^{-1} and high luminosity LHC (HL-LHC) with 3000 fb^{-1} of integrated luminosity. For $\tan\beta = 10$, the exclusion limits range up to $m_A \sim 1, 1.1$ and 1.4 TeV, respectively. These may be compared to the range of m_A values gleaned from a statistical analysis of the string landscape wherein m_A can range up to ~ 8 TeV.



check for updates

Citation: Baer, H.; Barger, V.; Tata, X.; Zhang, K. Prospects for Heavy Neutral SUSY HIGGS Scalars in the hMSSM and Natural SUSY at LHC Upgrades. *Symmetry* **2022**, *14*, 2061. <https://doi.org/10.3390/sym14102061>

Academic Editor: Alberto Ruiz Jimeno

Received: 8 September 2022

Accepted: 22 September 2022

Published: 3 October 2022

Publisher's Note: MDPI stays neutral with regard to jurisdictional claims in published maps and institutional affiliations.



Copyright: © 2022 by the authors. Licensee MDPI, Basel, Switzerland. This article is an open access article distributed under the terms and conditions of the Creative Commons Attribution (CC BY) license (<https://creativecommons.org/licenses/by/4.0/>).

Keywords: Higgs bosons; LHC; supersymmetry; naturalness

1. Introduction

The search for R -parity conserving supersymmetric (SUSY) particles at colliding beam experiments is plagued by the necessity to *pair produce* sparticles, and by the fact that the sparticle cascade decay terminates in the lightest SUSY particle (LSP), usually assumed to comprise at least a portion of the missing dark matter in the universe. The first of these thus requires enough energy to produce two rather than just one sparticle, while the second of these means that the sparticle invariant mass can not be directly reconstructed as a resonance. An alternative path to SUSY discovery at collider experiments is to search for the R -parity even neutral heavy Higgs bosons, the heavy scalar H and the pseudoscalar A . These particles can be produced singly as s -channel resonances and have the advantage in that their invariant mass can, in principle, be directly reconstructed (as was the case in discovery of the light scalar h).

In this paper, we examine production and decay of the heavy neutral scalar Higgs bosons of the MSSM in the most lucrative discovery channel $pp \rightarrow H, A \rightarrow \tau\bar{\tau}$. In previous phenomenological work [1–5], new scenarios were proposed for the m_A vs. $\tan\beta$ discovery plane which ensured that $m_h \simeq 125$ GeV while also respecting that LHC sparticle search limits were enforced, usually by assuming supersymmetry breaking in the multi-TeV regime. These constraints can in principle affect the regions of the heavy Higgs search planes which can be probed by current and forthcoming hadron colliders.

In the present work, we add to these constraints the condition that the magnitude of the weak scale also be *natural*. This is because natural SUSY models are in a sense more plausible than unnatural models [6]. For our naturalness criterion, we adopt the notion of practical naturalness [7]:

An observable $\mathcal{O} = o_1 + \dots + o_n$ is natural if all *independent* contributions to \mathcal{O} are comparable to or less than \mathcal{O} .

Here, we adopt the measured value of the Z-boson mass as representative of the magnitude of weak scale, where in the Minimal Supersymmetric Standard Model (MSSM) [8], the Z mass is related to Lagrangian parameters via the electroweak minimization condition

$$m_Z^2/2 = \frac{m_{H_d}^2 + \Sigma_d^d - (m_{H_u}^2 + \Sigma_u^u) \tan^2 \beta}{\tan^2 \beta - 1} - \mu^2 \quad (1)$$

where $m_{H_u}^2$ and $m_{H_d}^2$ are the Higgs soft breaking masses, μ is the (SUSY preserving) superpotential μ parameter and the Σ_d^d and Σ_u^u terms contain a large assortment of loop corrections (see Appendices of Ref's [9–11] for leading two-loop corrections). For natural SUSY models, the naturalness measure [12]

$$\Delta_{EW} \equiv |\text{maximal term on the right-hand-side of Equation (1)}|/(m_Z^2/2) \quad (2)$$

is adopted here where a value

$$\Delta_{EW} \lesssim 30 \quad (3)$$

fulfills the *comparable* condition of practical naturalness. For most SUSY benchmark models, the superpotential μ parameter is tuned to cancel against large contributions to the weak scale from SUSY breaking. Since the μ parameter typically arises from very different physics than SUSY breaking, e.g., from whatever solution to the SUSY μ problem that is assumed, (Twenty solutions to the SUSY μ problem are recently reviewed in Ref. [13].) then such a “just-so” cancellation seems highly implausible [6] (though not impossible) compared to the case where all contributions to the weak scale are $\sim m_{weak}$, so that μ (or any other parameter) need not be tuned.

There are several important implications of Equation (3) for heavy neutral SUSY Higgs searches.

- The superpotential μ parameter enters Δ_{EW} directly, leading to $|\mu| \lesssim 350$ GeV. This implies that for heavy Higgs searches with $m_{A,H} \gtrsim 2|\mu|$, then SUSY decay modes of H, A should typically be open. If these additional decay widths to SUSY particles are large, then the branching fraction to the $\tau\bar{\tau}$ discovery mode can be substantially reduced.
- For $m_{H_d} \gg m_{H_u}$, then m_{H_d} sets the heavy Higgs mass scale ($m_{A,H} \sim m_{H_d}$) while m_{H_u} sets the mass scale for $m_{W,Z,h}$. Then naturalness requires [14]

$$m_{A,H} \lesssim m_Z \tan \beta \sqrt{\Delta_{EW}}. \quad (4)$$

For $\tan \beta \sim 10$ with $\Delta_{EW} \lesssim 30$, then m_A can range up to ~ 5 TeV. For $\tan \beta \sim 40$, then m_A stays natural up to ~ 20 TeV (although for large $\tan \beta \gtrsim 20$, then bottom squark contributions to Σ_u^u become large and provide typically much stronger limits on natural SUSY spectra). Since most $H, A \rightarrow \tau\bar{\tau}$ searches and projected reach limits take place assuming a decoupled SUSY spectra, then such results can overestimate the collider heavy Higgs reach since in general the presence of $H, A \rightarrow SUSY$ decay modes will diminish the $H, A \rightarrow \tau\bar{\tau}$ branching fraction.

Using naturalness, in Section 2 we propose a new natural SUSY benchmark scenario $m_h^{125}(\text{nat})$ which is also consistent with expectations from the string landscape [15]. In Section 3, we discuss production and decay of heavy neutral Higgs bosons in the $m_h^{125}(\text{nat})$ scenario. In Section 4, we discuss signal event generation and SM backgrounds for the case of back-to-back (BtB) τ s in the transverse plane using the total transverse mass variable m_T^{tot} . In Section 5, we discuss signal and background for the acollinear tau pairs using the $m_{\tau\tau}$ variable. Including this signal channel can lead to a substantial increase in signal significance and so combined with the BtB τ s can give an increased collider reach in the m_A vs. $\tan \beta$ search plane. In Section 6, we present our reach of present LHC with 139 fb^{-1}

and also the projected reach of LHC Run3 and high-luminosity LHC (HL-LHC). Our conclusions reside in Section 7.

2. The Natural SUSY Higgs Search Plane

The mass of the light SUSY Higgs boson is given approximately by [16]

$$m_h^2 \simeq m_Z^2 \cos^2 2\beta + \frac{3g^2}{8\pi^2} \frac{m_t^4}{m_W^2} \left[\ln \frac{m_{\tilde{t}}^2}{m_t^2} + \frac{x_t^2}{m_{\tilde{t}}^2} \left(1 - \frac{x_t^2}{12m_{\tilde{t}}^2} \right) \right] \quad (5)$$

where $x_t = A_t - \mu \cot \beta$ and $m_{\tilde{t}}^2 \simeq m_{Q_3} m_{U_3}$ is the mean top squark mass. For a given value of $m_{\tilde{t}}^2$, then m_h^2 is maximal for $x_t^{max} = \pm \sqrt{6} m_{\tilde{t}}$.

2.1. Some Previous SUSY Higgs Benchmark Studies

In Ref. [1], a variety of SUSY Higgs search benchmark points were proposed, including 1. the m_h^{max} scenario where a value of x_t^{max} was chosen along with $m_{\tilde{g}} = 1500$ GeV and $m_{SUSY} \equiv m_{\tilde{t}} = 1$ TeV with $\mu = M_2 = 0.2$ TeV as a conservative choice which maximized the parameter space of the m_A vs. $\tan \beta$ plane available for new SUSY Higgs boson searches. Similarly, m_h^{mod+} and m_h^{mod-} scenarios were proposed with similar parameters except for more moderate $x_t = 1.6 m_{SUSY}$ and $x_t = -2.2 m_{SUSY}$ values. Light stop, light stau, τ -phobic and low m_H scenarios were proposed as well. Over time, all these benchmark models have become LHC-excluded since (at least) they all proposed $m_{\tilde{g}} \sim 1500$ GeV while after LHC Run 2 the ATLAS/CMS Collaborations require $m_{\tilde{g}} \gtrsim 2.2$ TeV [17,18].

In Ref. [4], an m_h^{125} benchmark model was proposed with $m_{SUSY} \sim 1.5$ TeV, $\mu = 1$ TeV and $m_{\tilde{g}} = 2.5$ TeV in accord with LHC Run 2 gluino mass constraints. The $x_t = 2.8$ TeV value was chosen to nearly maximize the value of m_h given the other parameters of the model. This model has almost all $H, A \rightarrow SUSY$ decay modes kinematically closed due to the heavy SUSY spectra so it closely resembles the type-II two-Higgs doublet model (2HDM) phenomenology [19]. An $m_h^{125}(\tilde{\tau})$ scenario (exemplifying bino-stau coannihilation) was selected with $\mu = 1$ TeV along with a $m_h^{125}(\tilde{\chi})$ scenario with $\mu = 180$ GeV, $M_1 = 160$ GeV and $M_2 = 180$ GeV so that H, A decay to many electroweakino states is allowed. Furthermore, an $m_h^{125}(align)$ model with specific *alignment without decoupling* [20,21] parameters with $\mu = 7.5$ TeV was chosen along with a m_H^{125} scenario where the heavy Higgs scalar was actually the 125 GeV Higgs boson. These scenarios would be hard pressed to explain why $m_{weak} \sim 100$ GeV due to the tuning needed for such large μ parameters. The exception is the $m_h^{125}(\tilde{\chi})$ scenario, although here the peculiar gaugino/higgsino mass choices seem at odds with most theory expectations (Gaugino mass unification is usually expected in models based on grand unification, but is also expected by the simple form of the supergravity (SUGRA) gauge kinetic function which depends typically on only a single hidden sector field in many string-inspired constructs.).

A somewhat different approach is taken in the model labelled $hMSSM$ [2,3,22]. In the $hMSSM$, by adopting a high m_{SUSY} scale and by neglecting some small radiative corrections to the Higgs mass matrix, then one may use m_h (along with m_A and $\tan \beta$) as an input parameter with Higgs mixing angle α , m_H and m_{H^\pm} as outputs. This ensures that $m_h = 125$ GeV is enforced throughout the remaining Higgs search parameter space. The adoption of a high value $m_{SUSY} \gtrsim 1$ TeV then makes this model look like the 2HDM, and sparticle mass spectra are effectively neglected. By combining $H, A \rightarrow \tau\bar{\tau}$ with $H, A \rightarrow t\bar{t}$ at lower $\tan \beta$, then it is claimed almost the entire m_A vs. $\tan \beta$ parameter space can be probed by HL-LHC for $m_A \lesssim 1$ TeV [3].

2.2. Status of Run 2 LHC Searches

The ATLAS Collaboration has reported on a search for $H, A \rightarrow \tau\bar{\tau}$ at CERN LHC Run 2 using 139 fb^{-1} of integrated luminosity at $\sqrt{s} = 13$ TeV [23]. The study focusses on back-to-back $\tau\bar{\tau}$ states where transverse opening angles $\Delta\phi(\tau_{had}\tau_{had}) > 155^\circ$ and $\Delta\phi(\tau_{lep}\tau_{had}) > 135^\circ$ are required. Mixed leptonic-hadronic ($\tau_{lep}\tau_{had}$) and hadronic-hadronic

$(\tau_{had}\tau_{had})$ final states are combined. The hadronic tau tagging efficiency in one or three charged prong τ -jets varies from 60 to 85%. The total transverse mass [24]

$$m_T^{tot} = \sqrt{(p_T^{\tau_1} + p_T^{\tau_2} + E_T^{miss})^2 - (\vec{p}_T^{\tau_1} + \vec{p}_T^{\tau_2} + \vec{E}_T^{miss})^2} \quad (6)$$

is measured and a fit to expected signal plus background is made to determine the presence of a signal. For the signal, the m_T^{tot} distribution is bounded from above by $m_T^{tot} < m_{H,A}$ and near this upper bound is where the signal-to-background significance is greatest. In this region, the dominant background comes from Drell-Yan $\gamma^*, Z \rightarrow \tau\bar{\tau}$ production. The signal sample is further divided by either the presence or absence of a tagged b -jet but the signal significance is dominated by the b -jet vetoed events. No signal is found, so the 95% CL exclusion limits are plotted in the m_A vs. $\tan\beta$ plane in the Bagnaschi et al. m_h^{125} scenario [4]. They find that for $\tan\beta \sim 10$, then $m_A \lesssim 1.1$ TeV is already excluded while for $\tan\beta \sim 50$, then $m_A \lesssim 2$ TeV is excluded.

The CMS collaboration has presented results of $H, A \rightarrow \tau\bar{\tau}$ searches using 35.9 fb⁻¹ of integrated luminosity [25]. The 95% CL exclusion limits are plotted in the m_A vs. $\tan\beta$ plane for the m_h^{mod+} and hMSSM scenarios. Further CMS analyses using the full Run 2 data set should be forthcoming.

2.3. Some Previous LHC Upgrade SUSY Higgs Reach Studies

In Ref. [26], the ATLAS and CMS collaborations presented expected reach plots for $H, A \rightarrow \tau\bar{\tau}$ for HL-LHC with either 3 or 6 ab⁻¹ of integrated luminosity and $\sqrt{s} = 14$ TeV. The results were a direct extrapolation of their previous search results from LHC Run 2. ATLAS with 3 ab⁻¹ expects to explore $m_A \lesssim 1500$ GeV for $\tan\beta = 10$ in the hMSSM scenario and up to $m_A \lesssim 1$ TeV in the m_h^{mod+} scenario. The plot upper limit of $m_A < 2250$ GeV precludes any limits for $\tan\beta \gtrsim 40$. With 3 ab⁻¹, the CMS collaboration expects to explore at 95% CL up to $m_A < 750$ GeV in the m_h^{mod+} scenario and up to $m_A \lesssim 1400$ GeV in the hMSSM scenario, both for $\tan\beta = 10$.

The HL-LHC and ILC sensitivity for heavy SUSY Higgs bosons was also estimated by Bahl et al. [5]. Their 95% CL exclusion using a combined ATLAS/CMS sensitivity (6 ab⁻¹) is to explore up to $m_A \lesssim 1500$ GeV for $\tan\beta = 10$ in the m_h^{125} scenario (heavy SUSY) and to $m_A \lesssim 1$ TeV in the $m_h^{125}(\tilde{\chi})$ scenario (light electroweakinos (EWinos)). They also explore some $m_{h,EFT}^{125}$ scenarios [27] at low $\tan\beta \sim 1-10$ which we will not consider.

2.4. The $m_h^{125}(nat)$ Higgs Search Benchmark

In this Subsection, we introduce a more plausible SUSY Higgs search benchmark model in that all its contributions to the weak scale are comparable to or less than the weak scale by a conservative factor of ~ 4 . This would be the class of natural SUSY models characterized by $\Delta_{EW} \lesssim 30$ [12]. These natural SUSY models can be found in several different guises:

1. The 2,3,4-extra parameter non-universal Higgs models NUHM2,3,4 which characterize what might be expected from dominant gravity-mediated SUSY breaking [9],
2. natural anomaly-mediated SUSY breaking [28] (nAMSB) wherein non-universal bulk soft terms allow for naturalness while maintaining $m_h \simeq 125$ GeV and
3. natural generalized mirage-mediation (nGMM) models [29] wherein soft terms are characterized by comparable anomaly- and gravity/moduli-mediated contributions. The nGMM model is expected to emerge [30] from KKLT moduli stabilization [31] and the string landscape [32].

For our benchmark models, it is perhaps easiest to settle on the more familiar gravity-mediated two-extra-parameter non-universal Higgs model NUHM2 [33,34] which is characterized by the parameter space

$$m_0, m_{1/2}, A_0, \tan\beta, m_{H_u}, m_{H_d} \quad (7)$$

where m_0 denotes the GUT scale matter scalar soft terms, $m_{1/2}$ are the unified gaugino masses, A_0 are common trilinear soft terms and $\tan \beta \equiv v_u/v_d$ is the usual ratio of Higgs field vevs. It is reasonable to have $m_{H_u} \neq m_{H_d} \neq m_0$ in gravity-mediation since the scalar mass soft terms in supergravity do not respect universality. However, a remnant $SO(10)$ local GUT symmetry may enforce the matter scalars of each generation to have a common mass $m_0(i)$, where $i = 1 - 3$ is a generation index. (In the landscape context, the first two generations are pulled to common upper bounds which yields a mixed decoupling/quasi-degeneracy solution to the SUSY flavor and CP problems [35]. The third generation is pulled up much less than the first two generations since it contributes more to the weak scale via the large Yukawa couplings.) The Higgs soft terms m_{H_u} and m_{H_d} are frequently traded for the weak scale parameters μ and m_A via the scalar potential minimization conditions. Thus, the parameter space of NUHM2

$$m_0, m_{1/2}, A_0, \tan \beta, \mu, m_A \tag{8}$$

is well-suited to Higgs searches since it allows for variable m_A and $\tan \beta$ as independent input parameters while also allowing the input of $\mu \lesssim 350$ GeV which is required by naturalness in Equation (1).

Using NUHM2, we adopt the following natural SUSY benchmark Higgs search scenario:

$$m_h^{125}(\text{nat}) : m_0 = 5 \text{ TeV}, m_{1/2} = 1.2 \text{ TeV}, A_0 = -1.6m_0, \tan \beta, \mu = 250 \text{ GeV and } m_A. \tag{9}$$

The $m_h^{125}(\text{nat})$ benchmark model spectra is shown in Table 1 for $\tan \beta = 10$ and $m_A = 2$ TeV. We adopt the computer code Isajet [36] featuring Isasugra [37] for spectra generation. (The value of $\sigma^{SI}(\tilde{\chi}_1^0, p)$ from Table 1 appears to be in conflict with recent results from the LZ experiment [38] (see also results from Xenon1T [39] and PandaX-II [40]) on direct detection of WIMP scattering on their liquid Xe target, even in the case where the relic neutralinos are thermally underproduced with the remainder of dark matter composed of, e.g., axions [41]. This is of course a model-dependent result and entropy dilution from late decaying saxion [42] or moduli [43] fields could further reduce the neutralino relic abundance bringing the BM point into accord with limits from direct detection [44].) The SUSY Higgs boson masses are computed using renormalization-group (RG) improved third generation fermion/sfermion loop corrections [45]. The RG improved Yukawa couplings include full threshold corrections [46] which account for leading two-loop effects [47]. From the Table, we note that $m_h = 124.7$ GeV and $\Delta_{EW} = 22$. Recent versions of FeynHiggs [48] predict m_h values closer to Isasugra than past versions, and for the $m_h^{125}(\text{nat})$ benchmark point we find from FeynHiggs 2.18.1 that $m_h = 125.3 \pm 1.3$ GeV, in close accord with Isasugra.

In Figure 1a, we show regions of light Higgs mass m_h in the m_A vs. $\tan \beta$ plane for the $m_h^{125}(\text{nat})$ benchmark scenario. From the plot, we can see that the value of m_h is indeed very close to 125 GeV throughout the entire plane except for very low $\tan \beta \lesssim 6$ where m_h dips below 123 GeV. In Figure 1b), we show regions of EW naturalness measure Δ_{EW} . We see that in the region of $\tan \beta: 1-15$, then $\Delta_{EW} \lesssim 30$ even for m_A extending out as high as 5 TeV. For larger $\tan \beta \gtrsim 20$, then Δ_{EW} moves to $\sim 45-90$ mainly because the b - and τ -Yukawa couplings grow and lead to large $\Sigma_{ii}^u(\tilde{b}, \tilde{\tau})$ terms.

Table 1. Input parameters (TeV) and masses (GeV) for the $m_h^{125}(\text{nat})$ SUSY benchmark point from the NUHM2 model with $m_t = 173.2$ GeV using Isajet 7.88 [36].

Parameter	$m_h^{125}(\text{nat})$
m_0	5 TeV
$m_{1/2}$	1.2 TeV
A_0	-8 TeV
$\tan \beta$	10

Table 1. Cont.

Parameter	m_h^{125} (nat)
μ	250 GeV
m_A	2 TeV
$m_{\tilde{g}}$	2830 GeV
$m_{\tilde{u}_L}$	5440 GeV
$m_{\tilde{u}_R}$	5561 GeV
$m_{\tilde{e}_R}$	4822 GeV
$m_{\tilde{t}_1}$	1714 GeV
$m_{\tilde{t}_2}$	3915 GeV
$m_{\tilde{b}_1}$	3949 GeV
$m_{\tilde{b}_2}$	5287 GeV
$m_{\tilde{\tau}_1}$	4746 GeV
$m_{\tilde{\tau}_2}$	5110 GeV
$m_{\tilde{\nu}_\tau}$	5107 GeV
$m_{\tilde{\chi}_1^\pm}$	261.7 GeV
$m_{\tilde{\chi}_2^\pm}$	1020.6 GeV
$m_{\tilde{\chi}_1^0}$	248.1 GeV
$m_{\tilde{\chi}_2^0}$	259.2 GeV
$m_{\tilde{\chi}_3^0}$	541.0 GeV
$m_{\tilde{\chi}_4^0}$	1033.9 GeV
m_h	124.7 GeV
$\Omega_{\tilde{z}_1}^{std} h^2$	0.016
$BF(b \rightarrow s\gamma) \times 10^4$	3.1
$BF(B_s \rightarrow \mu^+ \mu^-) \times 10^9$	3.8
$\sigma^{SI}(\tilde{\chi}_1^0, p)$ (pb)	2.2×10^{-9}
$\sigma^{SD}(\tilde{\chi}_1^0, p)$ (pb)	2.9×10^{-5}
$\langle \sigma v \rangle _{v \rightarrow 0}$ (cm ³ /s)	1.3×10^{-25}
Δ_{EW}	22

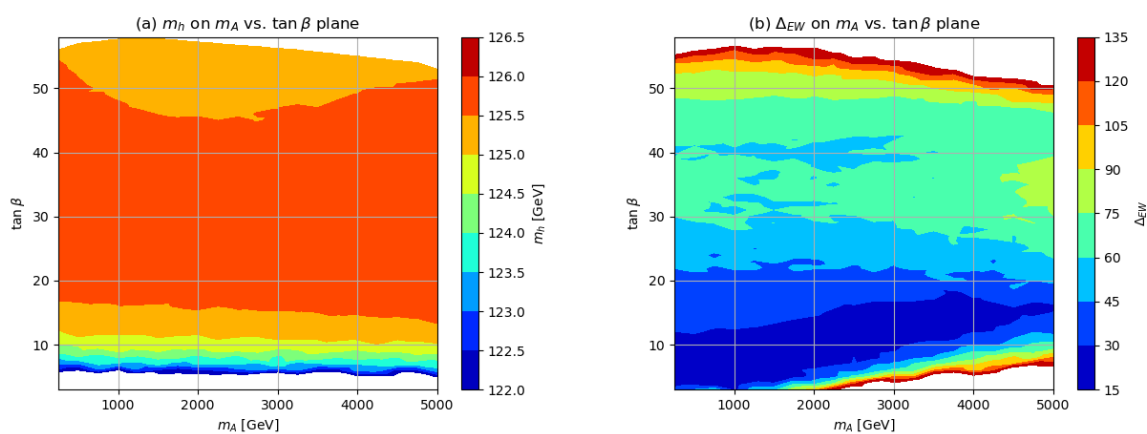


Figure 1. (a) Contours of m_h in the m_A vs. $\tan \beta$ plane using the m_h^{125} (nat) scenario from the NUHM2 model with $m_0 = 5$ TeV, $m_{1/2} = 1.2$ TeV, $A_0 = -8$ TeV and $\mu = 250$ GeV. (b) Regions of electroweak naturalness measure Δ_{EW} in the same plane as (a).

3. Production and Decay of H, A in the m_h^{125} (nat) Scenario

3.1. H and A Production Cross Sections in the m_h^{125} (nat) Scenario

The s -channel resonance production of the H and A bosons takes place mainly via gg and $q\bar{q}$ (mainly $b\bar{b}$) fusion reactions at hadron colliders. The total H and A production cross sections are shown in the m_A vs. $\tan\beta$ plane in Figure 2 for $\sqrt{s} = 14$ TeV pp collisions—as are expected at CERN LHC Run 3 and at high-luminosity LHC (HL-LHC) where of order 300 fb^{-1} (for Run 3) and 3000 fb^{-1} (for HL-LHC) of integrated luminosity is expected to be obtained. For the cross sections, we use the computer code SusHi [49] which contains contributions up to NNLO in perturbative QCD. The cross sections range from over 10^4 fb at low $m_{H,A} \sim 400 \text{ GeV}$ down to $\sigma(pp \rightarrow H, A) < 1 \text{ fb}$ for $m_{H,A} \sim 2 \text{ TeV}$, and they increase somewhat with increasing $\tan\beta$ where production via $b\bar{b}$ fusion is enhanced.

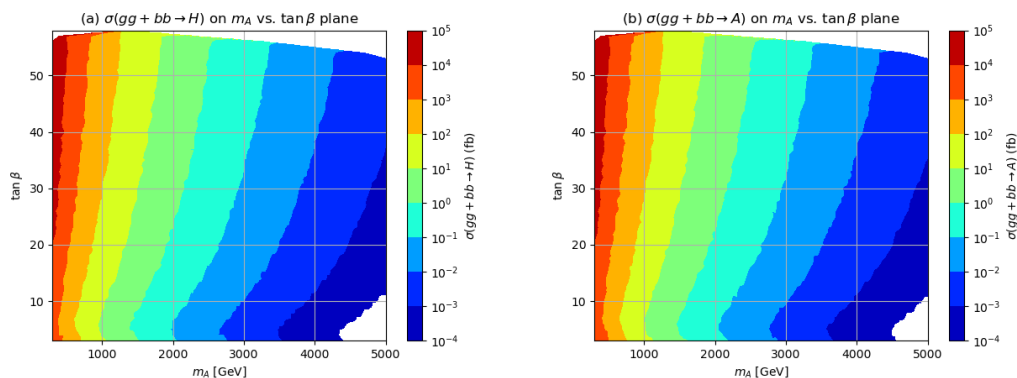


Figure 2. The total cross section for (a) $pp \rightarrow H$ and (b) $pp \rightarrow A$ at $\sqrt{s} = 14$ TeV using the SusHi code [49].

3.2. H and A Branching Fractions in the m_h^{125} (nat) Scenario

It is sometimes claimed in the literature that the tree-level production and decay rates for the H and A bosons depend only on m_A and $\tan\beta$, and indeed search limits for the heavy Higgs bosons are typically presented in the m_A vs. $\tan\beta$ plane, following the early pioneering work by Kunszt and Zwirner [50]. While this is true for the (non-supersymmetric) 2HDM, it is not true for the MSSM, where the importance of tree level SUSY Higgs boson decays to SUSY particles was first emphasized in [51–53]. In the 2HDM, decays of H and A to the heaviest available fermion pairs will typically dominate, with decays to $b\bar{b}$ and $\tau\bar{\tau}$ enhanced at large $\tan\beta$. However, in SUSY models there is a direct gauge coupling

$$\mathcal{L} \ni -\sqrt{2} \sum_{i,A} S_i^\dagger g t_A \bar{\lambda}_A \psi_i + H.c. \tag{10}$$

where S_i labels various matter and Higgs scalar fields, ψ_i is the fermionic superpartner of S_i and λ_A is the gaugino with gauge index A . Furthermore, g is the corresponding gauge coupling for the gauge group in question and the t_A are the corresponding gauge group matrices. Letting S_i be the Higgs scalar fields, we see there is an unsuppressed coupling of the Higgs scalars to gaugino plus higgsino. This coupling can lead to dominant SUSY Higgs boson decays to SUSY particles when the gaugino-plus-higgsino decay channel is kinematically unsuppressed.

In Figure 3, we plot the $H \rightarrow \tau\bar{\tau}$ branching fractions as color-coded regions in the m_A vs. $\tan\beta$ plane for (a) the hMSSM and (b) for our m_h^{125} (nat) BM scenario. For the hMSSM, we use the computer code 2HDMC [54] with $m_h = 125 \text{ GeV}$ throughout the m_A vs. $\tan\beta$ plane but with decoupled sparticles. We use the “Physical mass input set”. With the potential parameters λ_i as in the tree-level MSSM except λ_2 , which includes a correction term to bring the light CP-even higgs mass to be 125 GeV, the only free physical inputs left are then just m_A and $\tan\beta$. From frame (a), we see as expected that for the

hMSSM, the $BF(H \rightarrow \tau\bar{\tau})$ increases with $\tan\beta$. It also increases slightly as m_A increases since the τ Yukawa coupling f_τ increases slightly with scale choice. In frame (b) for the $m_h^{125}(\text{nat})$ case, we again see an increasing branching fraction as $\tan\beta$ increases, but now as m_A (and hence m_H) increases, various SUSY decay modes to EWinos open up, especially around $m_A \sim 1200$ GeV where decays to gaugino-plus-higgsino become accessible. We see the $BF(H \rightarrow \tau\bar{\tau})$ can drop from 12% on the left-side of the plot down to just a few percent on the right-hand-side. This is due to the fact that the decay to EWinos ultimately dominates the heavy Higgs branching fraction [55,56]. There is also a glitch apparent at around $m_A \sim 2500$ GeV in the contours. This occurs because we include SUSY threshold corrections to the Yukawa couplings which are implemented at the scale $m_{SUSY}^2 = m_{\tilde{t}_1} m_{\tilde{t}_2}$ and so the Yukawa couplings have a slight discontinuity (see, e.g., Figure 6 of Ref. [57]).

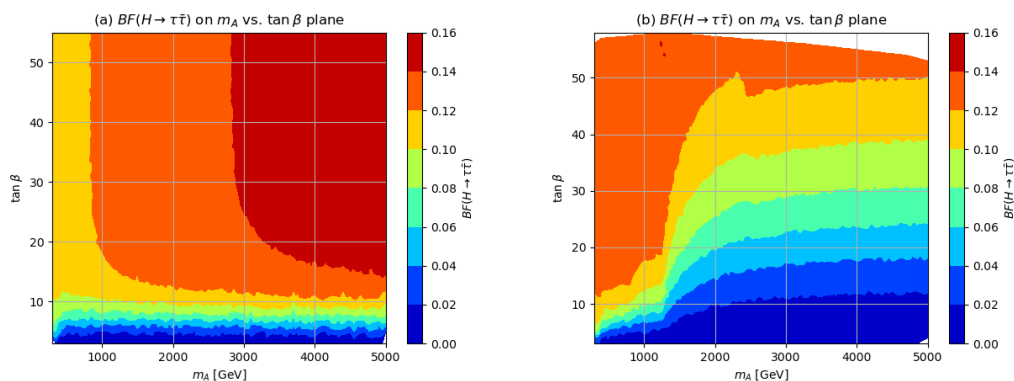


Figure 3. Branching fraction of $H \rightarrow \tau\bar{\tau}$ in the (a) hMSSM and (b) in the $m_h^{125}(\text{nat})$ benchmark case in the m_A vs. $\tan\beta$ plane.

It is also helpful to show the explicit $BF(H \rightarrow \tau\bar{\tau})$ vs. m_A for two specific choices of $\tan\beta = 10$ and 40 for the (a) hMSSM and (b) the $m_h^{125}(\text{nat})$ model in Figure 4. For the hMSSM, we again see the slight increase with increasing m_A , although the BFs stay in the vicinity of 10–15%. For the $m_h^{125}(\text{nat})$ case, we see the sharp drop off in $BF(H \rightarrow \tau\bar{\tau})$ as various $H \rightarrow E\text{Winos}$ thresholds are passed: then, ultimately the branching fraction drops below 2% for large m_A .

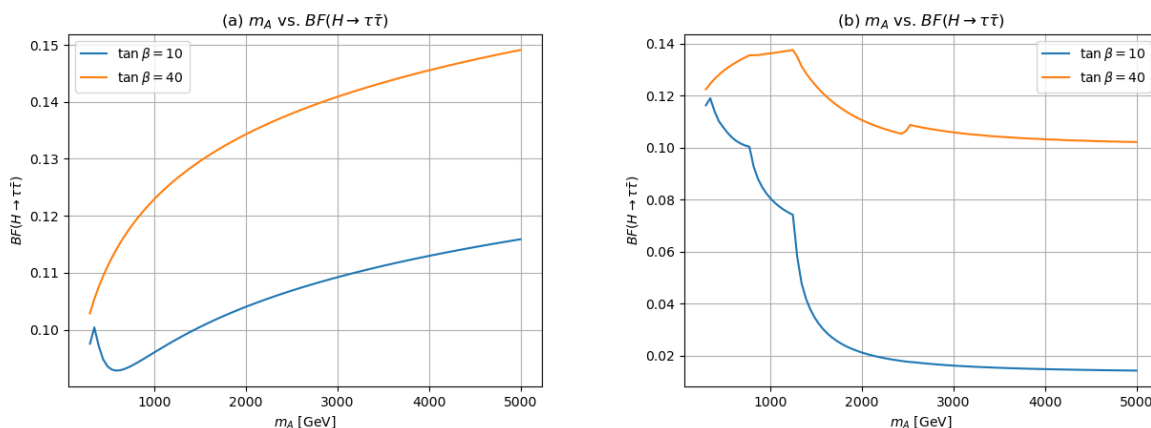


Figure 4. Branching fraction of $H \rightarrow \tau\bar{\tau}$ in the (a) hMSSM and (b) in the $m_h^{125}(\text{nat})$ benchmark case vs. m_A for $\tan\beta = 10$ and 40 .

Similar behavior is shown in Figure 5a,b for the $A \rightarrow \tau\bar{\tau}$ branching fraction: it has a slight increase with increasing m_A for the hMSSM case but suffers sharp drops in the $m_h^{125}(\text{nat})$ case due to the turn on of A decay to gaugino-plus-higgsino. This will affect the reach plots in a substantial way.

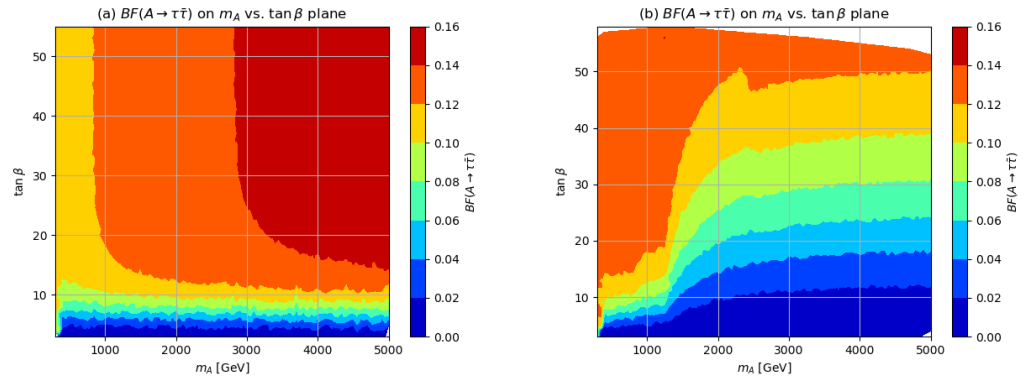


Figure 5. Branching fraction of $A \rightarrow \tau\bar{\tau}$ in the (a) hMSSM and (b) in the $m_h^{125}(\text{nat})$ benchmark case in the m_A vs. $\tan\beta$ plane.

The corresponding plots of $BF(A \rightarrow \tau\bar{\tau})$ vs. m_A for $\tan\beta = 10$ and 40 are shown in Figure 6. The behavior is rather similar to that already explained for the H decay.

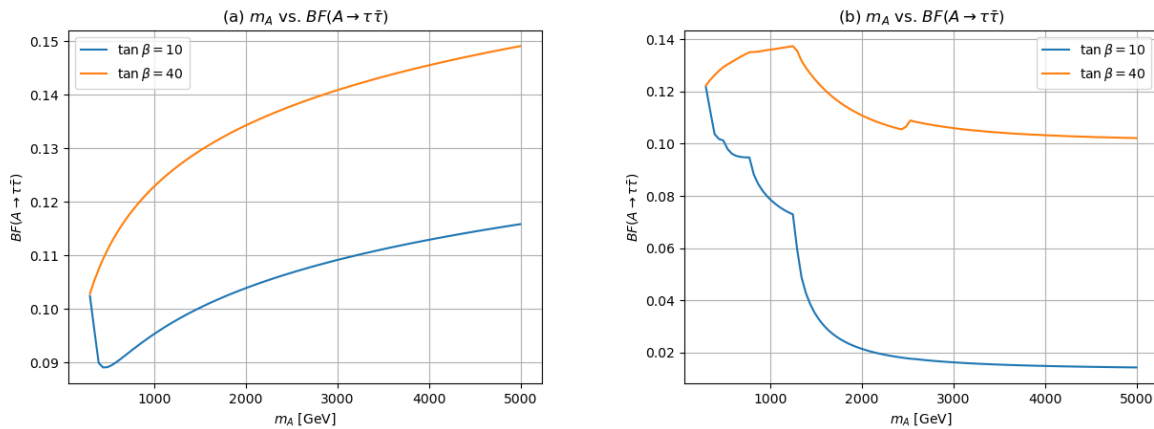


Figure 6. Branching fraction of $A \rightarrow \tau\bar{\tau}$ in the (a) hMSSM and (b) in the $m_h^{125}(\text{nat})$ benchmark case vs. m_A for $\tan\beta = 10$ and 40 .

4. Signal from Back-to-Back $\tau\bar{\tau}$ via m_T

In this Section, we present details from our event generation calculations for the $H, A \rightarrow \tau\bar{\tau}$ signal with nearly back-to-back (BtB) τ s. For signal and background event generation, we adopt the Pythia 8.07 event generator [58] interfaced with the Delphes toy detector simulation [59]. For signal, we generate $pp \rightarrow H, A \rightarrow \tau\bar{\tau}$ events with the total cross section adjusted to the SusHi NNLO result. For SM backgrounds, we generate $q\bar{q} \rightarrow \gamma^*, Z \rightarrow \tau\bar{\tau}$ (Drell-Yan), $t\bar{t}$ and VV production where $VV = W^+W^-, W^\pm Z$ and ZZ .

For jet finding, we use the Delphes FASTJET jet finder. The FASTJET jet finder requires $p_T(\text{jet}) > 25$ GeV and ΔR between jets as $\Delta R_{jj} > 0.4$. We also require $|\eta_{\text{jet}}| < 2.5$. Delphes includes a hadronic τ -jet finding tool which we also use which identifies one-and-three charged prong jets as tau jets provided the tau is within $\Delta R = 0.4$ of the jet in question. The Delphes τ -jet identification efficiency is found to be in the 50% range which is well below the ATLAS quoted τ -jet efficiency ID which is at the 75% level. We also use the Delphes b-tag algorithm and the Delphes isolated lepton tag which requires $\Delta R(l, l) > 0.3$ with $|\eta(e, \mu)| < 2.5$.

The $\tau_{\text{had}}\tau_{\text{had}}$ channel are selected by single- τ trigger p_T cut of 160 GeV. Events contain at least two τ_{had} identified by the Delphes tau-tag algorithm. The two tau τ_{had} candidates must have opposite electric charge.

The $\tau_{lep}\tau_{had}$ channel are selected using single-electron and single-muon triggers with p_T threshold of 30 GeV. The events contain exactly one isolated lepton and at least one τ_{had} candidate. The isolated lepton and the τ_{had} candidate must have opposite electric charge. Furthermore, we rejected the events that the isolated lepton and the τ_{had} candidate have an invariant mass between 80 GeV and 110 GeV to reduce the background contribution from $Z \rightarrow ee$.

The events from either channel are further divided into categories of the b -tag for events containing at least one b -jet and the b -veto for events containing no b -jets.

After selecting for candidate ditau events, we plot in Figure 7 the transverse opening angle $\Delta\phi(\tau\bar{\tau})$ from our signal and BG events for our $m_h^{125}(\text{nat})$ benchmark point with $m_A = 1$ and 2 TeV and $\tan\beta = 10$ and 40. Both the DY background and the signal events rise to a peak at 180° indicating that these events are mostly back-to-back in the transverse plane as expected. The ditau opening angle from $t\bar{t}$ and VV are rather less pronounced at $\Delta\phi \sim 180^\circ$.

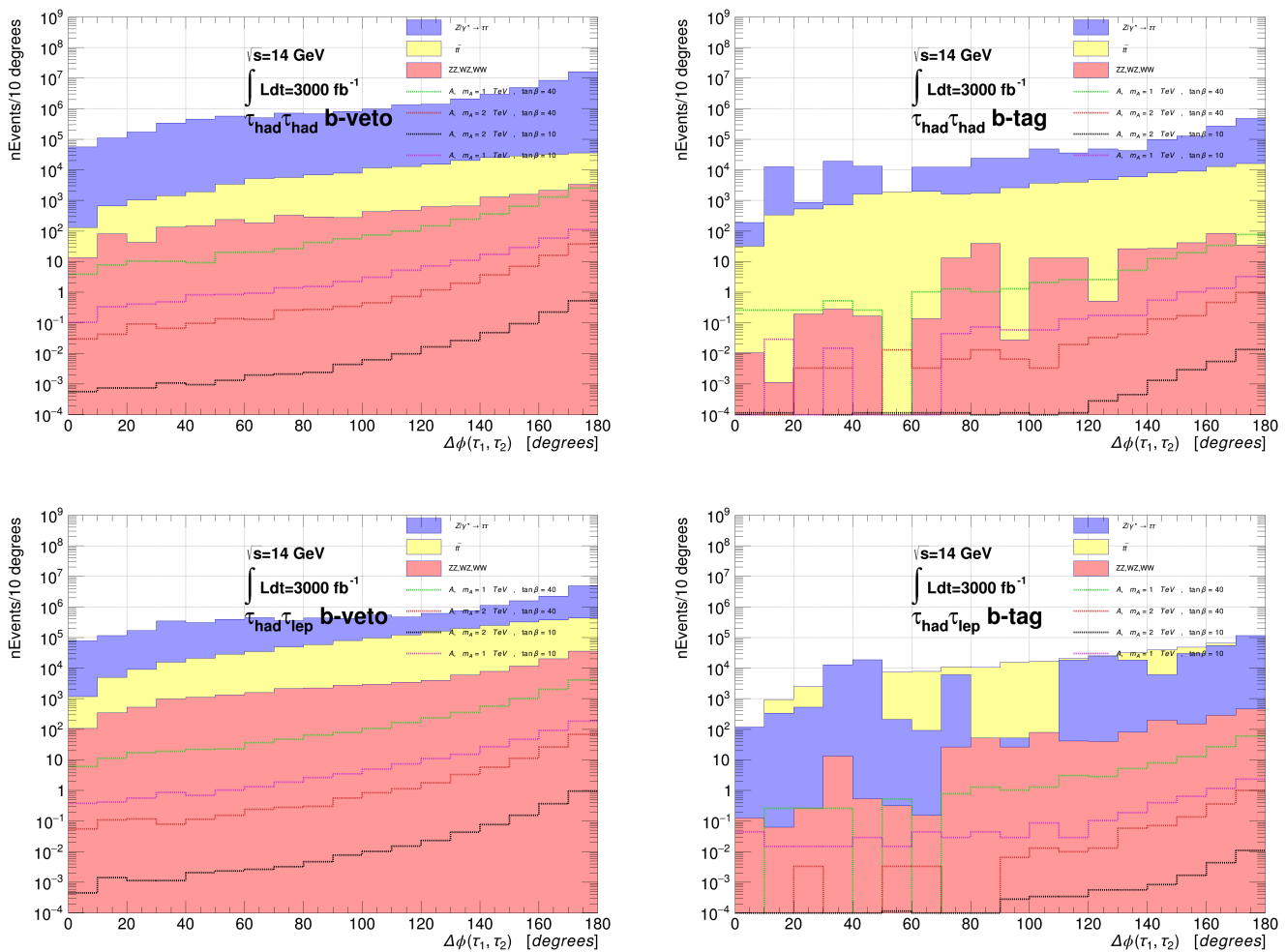


Figure 7. Distribution in transverse ditau opening angle $\Delta\phi(\tau\tau)$ for our $m_h^{125}(\text{nat})$ benchmark scenario with $\tan\beta = 10$ and $m_A = 1$ and 2 TeV.

We next divide our signal into BtB ditau events, where $\Delta\phi(\tau\tau) > 155^\circ$ (this Section) or non-BtB (acollinear) ditau where $\Delta\phi(\tau\tau) < 155^\circ$ (Section 5).

Then we plot the total transverse mass variable m_T^{tot} as shown in Figure 8. From the plot, we see that the signal distributions rise to a peak around $m_T \sim 0.8m_A$ and then fall off sharply for $m_T \gtrsim m_A$ due to kinematics (the cutoff is not completely sharp due to

considerable smearing entering into the signal distributions). The SM backgrounds are all peaked below $m_T \sim 500$ GeV and have falling distributions for increasing values of m_T^{tot} .

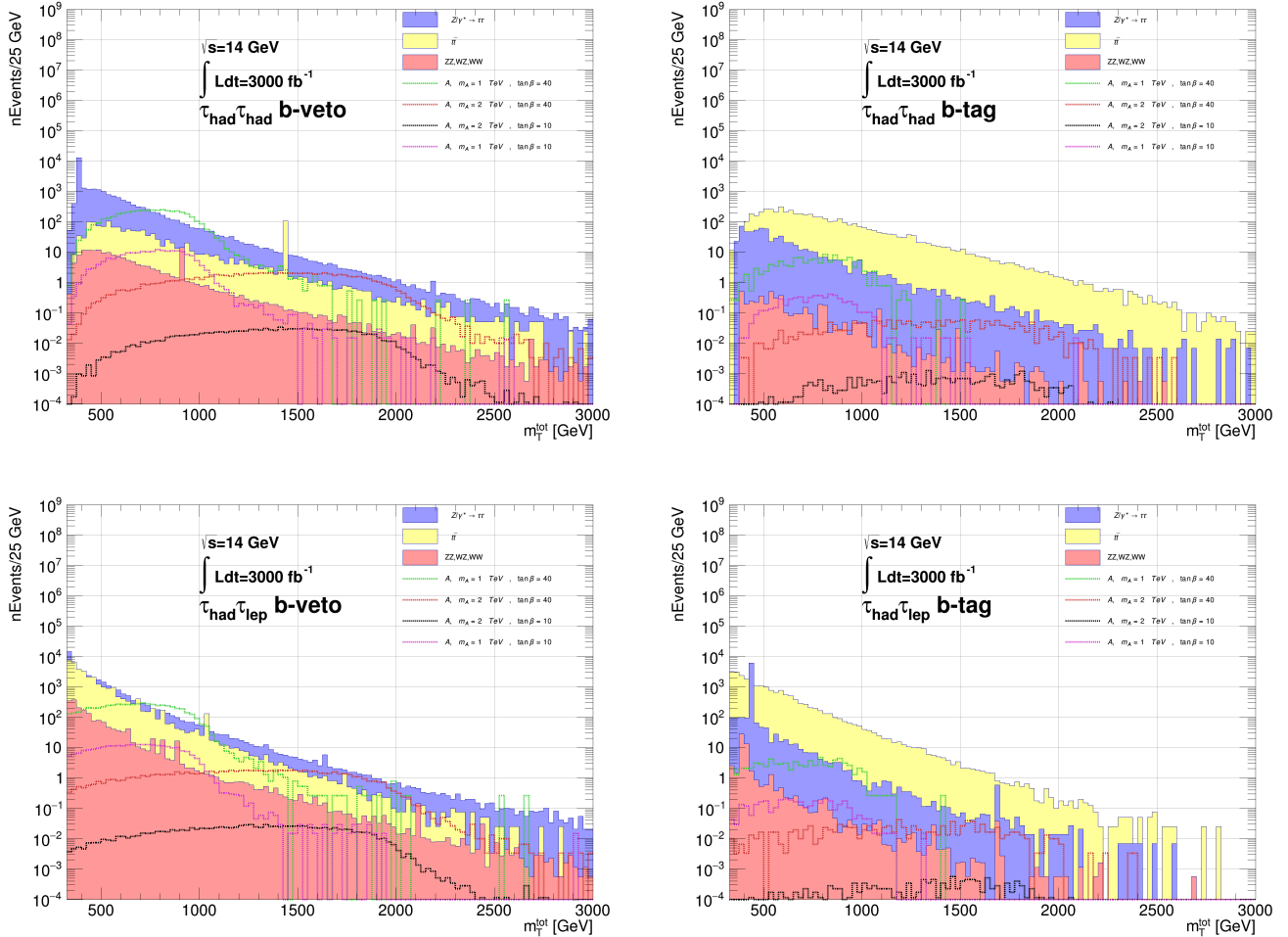


Figure 8. Distribution in m_T^{tot} for ditau events with $\Delta\phi(\tau\tau) > 155^\circ$ for our $m_h^{125}(\text{nat})$ benchmark scenario with $\tan\beta = 10$ and $m_A = 1$ and 2 TeV after cuts listed in the text.

5. Signal from Acollinear $\tau\bar{\tau}$ via $m_{\tau\tau}$

For acollinear ditau events (non-BtB), we require the transverse ditau opening angle $\Delta\phi(\tau\tau) < 155^\circ$ so that this data set is orthogonal to the back-to-back ditau set. For the acollinear ditau events, we also require the presence of an additional jet in the event besides the τ_{had} jets (usually an initial-state-radiation (ISR) jet in the case of signal events): $n_{jets} \geq 1$. For this configuration, then we are able to use the tau-tau invariant mass reconstruction trick since once \vec{E}_T^{miss} is known, and we assume the neutrinos from each tau decay are collinear with the parent tau direction, then the ditau invariant mass can be solved for. Since the taus are ultra-relativistic, the daughter visible decay products and the associated neutrinos are all boosted in the direction of the parent τ momentum. In the approximation that the visibles (vis) and the neutrinos from the decay of each tau are all exactly collimated in the tau direction, we can write the momentum carried off by the neutrinos from the decay $\tau_1 \rightarrow vis_1\nu$ of the first tau as $\zeta_1\vec{p}_T(vis_1)$ and likewise for the second tau. Momentum conservation in the transverse plane requires

$$-\vec{p}_T(j) = (1 + \zeta_1)\vec{p}_T(vis_1) + (1 + \zeta_2)\vec{p}_T(vis_2). \quad (11)$$

Since this is really two independent equations (recall we require $p_T(j) > 25$ GeV), it is possible to use the measured values of the jet and visible-tau-decay momenta to solve these to obtain ξ_1 and ξ_2 , event-by-event. It is simple to check that in the approximation of collinear tau decay, the squared mass of the di-tau system is given by

$$m_{\tau\tau}^2 = (1 + \xi_1)(1 + \xi_2)m_{vis_1vis_2}^2 \quad (12)$$

For ditau plus jet events from H, A -decay to taus, we expect $\xi_i > 0$ and $m_{\tau\tau}^2$ to peak at $m_{H,A}^2$. Moreover, for these events, the missing energy vector will usually point in between the two $\tau(vis)$ momentum vectors in the transverse plane. In contrast, for backgrounds where E_T^{miss} arises from neutrinos from decays of heavy SM particles (t, W, Z), the visible and E_T^{miss} directions are uncorrelated and the E_T^{miss} -vector may point well away, or even backwards, from one of the leptons so that one (or both) $\xi_i < 0$.

Then we can plot the $m_{\tau\tau}$ distribution, as is shown in Figure 9 for $\tan\beta = 10$ and 40 and for (a) $m_A = 1$ TeV and (b) $m_A = 2$ TeV. From the plot, the DY distribution shows a remnant peak at $m_Z = 91.2$ GeV while $t\bar{t}$ and VV are peaked below 500 GeV. In contrast, the $A \rightarrow \tau\bar{\tau}$ signal distributions are peaked at $m_{\tau\tau} \sim m_A$ with a width that arises from smearing effects and non-exact-collinearity of the τ decay products.

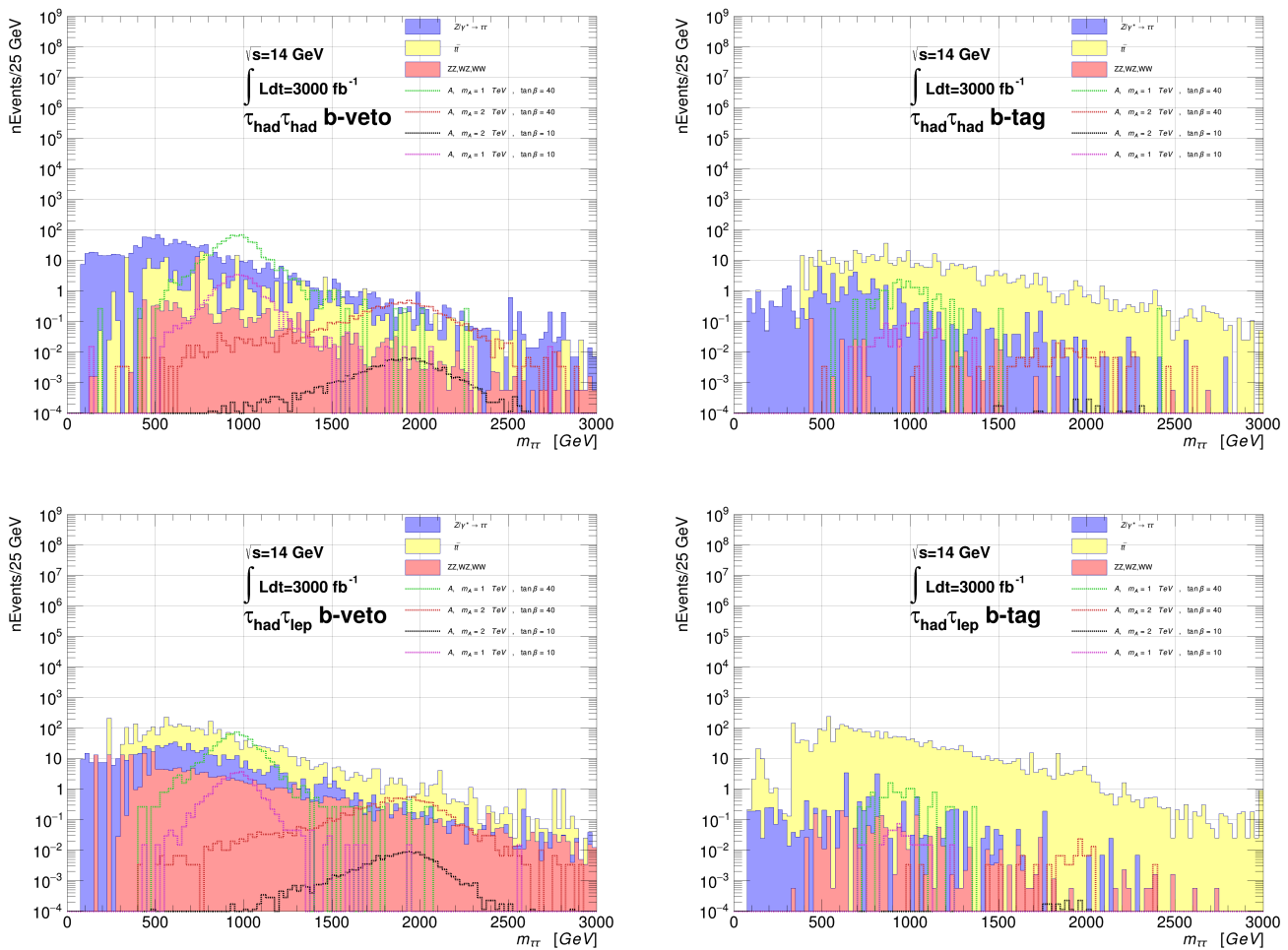


Figure 9. Distribution in $m_{\tau\tau}$ for ditau events with $\Delta\phi(\tau\tau) < 155^\circ$ and $n_{jet} \geq 1$ for our $m_h^{125}(\text{nat})$ benchmark scenario with $\tan\beta = 10$ and a) $m_A = 1$ and b) $m_A = 2$ TeV after cuts listed in the text.

To illustrate some numerics of our results, in Table 2 we list the resultant signal and background cross sections (in fb) after all cuts for the cases of $pp \rightarrow H, A \rightarrow \tau\bar{\tau}$

at $\sqrt{s} = 14$ TeV for $\tan \beta = 10$ and $m_A = 1$ TeV, for both the hMSSM and the $m_h^{125}(\text{nat})$ scenario. From the Table, we see that, as expected, the surviving signal after cuts from the $m_h^{125}(\text{nat})$ scenario is somewhat diminished from the hMSSM case due to the diminished branching fractions $BF(H, A \rightarrow \tau\bar{\tau})$. Furthermore, the two signal channels from H and from A production are nearly comparable. The dominant background comes from $\gamma^*, Z \rightarrow \tau\bar{\tau}$ while $t\bar{t}$ and VV are smaller but still significant. The signal is quite smaller in the acollinear channel than in the BtB channel. However, this is compensated for somewhat by smaller backgrounds in the acollinear channel than in the BtB channel, which makes the acollinear channel to have a much better S/B ratio than the BtB channel.

Table 2. Cross section (fb) after optimized cuts for the various signal and background processes from pp collisions at $\sqrt{s} = 14$ TeV and $\tan \beta = 10$ and $m_A = 1$ TeV.

Process	Back-to-Back (BtB)	Acollinear
$H \rightarrow \tau\bar{\tau}(\text{hMSSM})$	0.197	0.024
$A \rightarrow \tau\bar{\tau}(\text{hMSSM})$	0.222	0.027
$H \rightarrow \tau\bar{\tau}(\text{SUSY})$	0.140	0.017
$A \rightarrow \tau\bar{\tau}(\text{SUSY})$	0.162	0.020
$\gamma^*, Z \rightarrow \tau\bar{\tau}$	23.33	0.586
$t\bar{t}$	19.95	2.112
VV	0.663	0.069
$total(BG)$	43.94	2.767

6. Reach of LHC3 and HL-LHC for $H, A \rightarrow \tau\bar{\tau}$

After settling on cuts for the BtB and acollinear ditau signals, it is possible to plot reach plots in terms of exclusion limits or discovery sensitivity for $pp \rightarrow H, A \rightarrow \tau\bar{\tau}$ in the m_A vs. $\tan \beta$ plane.

For the exclusion plane, the upper limits for exclusion of a signal are set at the 95% CL and assume the true distribution one observes in experiment corresponds to background only. They are then computed using a modified frequentist CL_s method [60] with the profile likelihood ratio as the test statistic.

For the discovery plane, we use 5σ to denote the discovery and assume the true distribution one observes in experiment corresponds to signal-plus-background. Then we test this against the background only distribution to see if the background only hypothesis could be rejected at a 5σ level. Specifically, we use the binned m_T^{tot} distribution (Figure 8) for the BtB events and the $m_{\tau\tau}$ distribution (Figure 9) for acollinear events to obtain the exclusion/discovery limits.

In both the exclusion plane and the discovery plane, the asymptotic approximation for getting the median significance is used [61]. The systematic uncertainty is assumed to be 1σ of the corresponding statistical uncertainty, which is a very conservative rule-of-thumb estimate.

6.1. Exclusion Plane

As a first step, to compare with the ATLAS reach of upper limits obtained in their Run 2 search with 139 fb^{-1} , we plot our corresponding exclusion limit in Figure 10. For this plot, we use only the BtB signal in the hMSSM where m_h is set to 125 GeV, which should compare well with the m_h^{125} scenario used by ATLAS which contains sparticles at or around 2 TeV, i.e., presumably SUSY decay modes are closed for most m_A values shown in the plot. From Figure 10, we see our expected 95% CL exclusion extends to $m_A \sim 0.9$ TeV for $\tan \beta = 10$ which compares favorably with ATLAS. For $\tan \beta = 40$, we obtain a 95% CL exclusion of $m_A \sim 1.9$ TeV, which is somewhat better than the ATLAS expected result of $m_A \sim 1.8$ TeV.

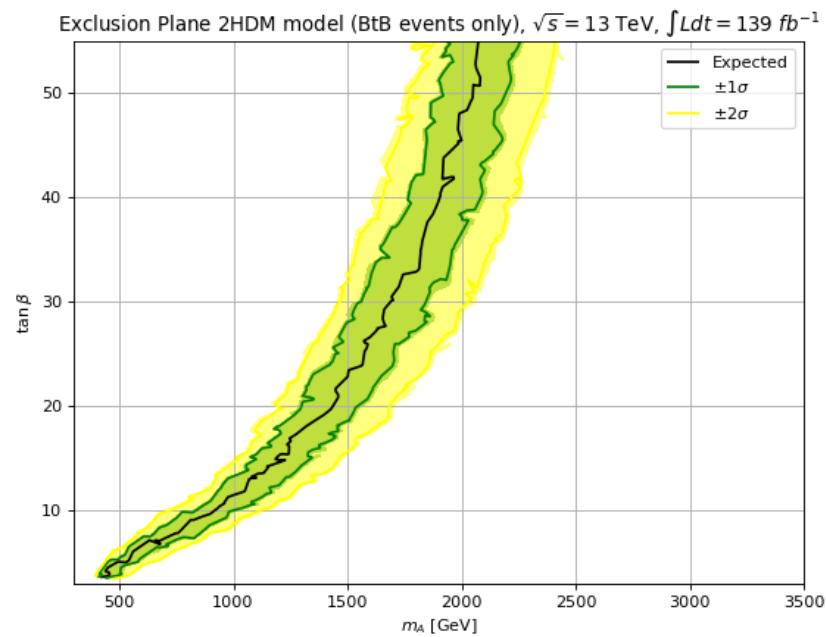


Figure 10. The 95% CL upper limits with $\sqrt{s} = 13$ TeV and 139 fb^{-1} for $H, A \rightarrow \tau\bar{\tau}$ using BtB signal only in the hMSSM.

In Figure 11, we plot in frame (a) our expected Run 2 exclusion assuming 139 fb^{-1} using the combined BtB and acollinear signal channels in the hMSSM. The exclusion limit extends to $m_A \sim 0.95$ TeV for $\tan\beta = 10$ and to $m_A \sim 1.95$ TeV for $\tan\beta = 40$. For frame (b), for the $m_h^{125}(\text{nat})$ scenario, then the corresponding 139 fb^{-1} reach extends to $m_A \sim 0.8$ TeV for $\tan\beta = 10$ and to $m_A \sim 1.8$ TeV for $\tan\beta = 40$.

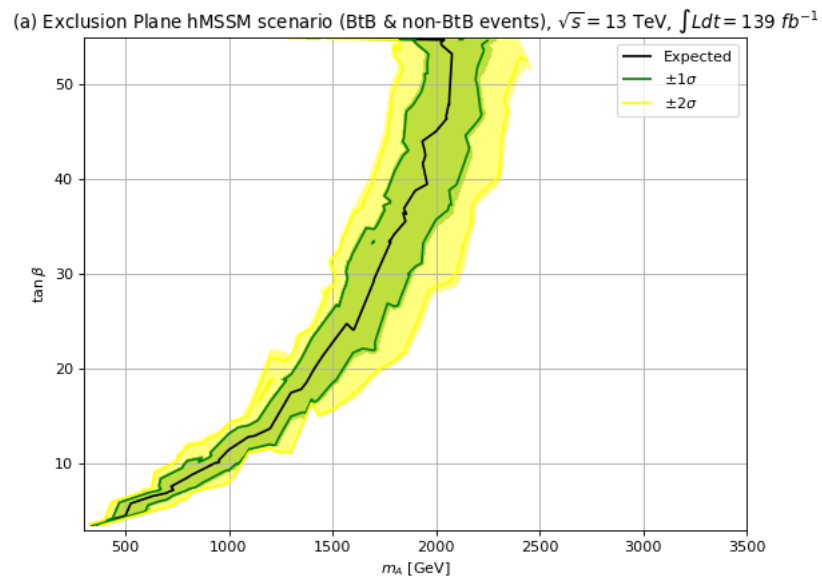


Figure 11. Cont.

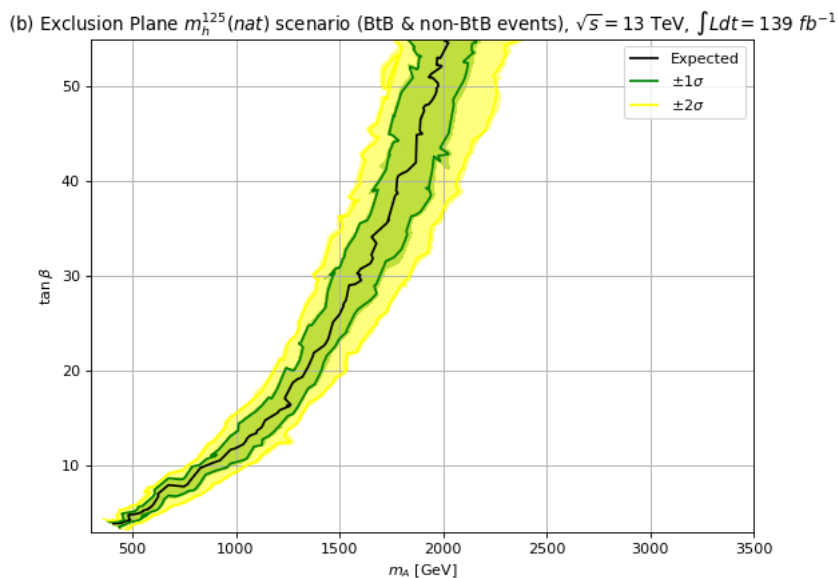


Figure 11. The 95% CL upper limits with $\sqrt{s} = 13$ TeV and 139 fb^{-1} for $H, A \rightarrow \tau\bar{\tau}$ in the (a) the hMSSM and (b) the $m_h^{125}(\text{nat})$ scenario.

In Figure 12, we present our projected future exclusion plots, this time for LHC collisions at $\sqrt{s} = 14$ TeV with 300 fb^{-1} of integrated luminosity, as would be expected from LHC Run 3. Here, we use both the BtB and acollinear signals. For Run 3, we see in frame (a) for the hMSSM with $\tan \beta = 10$, the 95% CL exclusion extends out to $m_A \sim 1.1$ TeV while the $\tan \beta = 40$ exclusion extends to $m_A \sim 2.3$ TeV. For the frame (b) case with the $m_h^{125}(\text{nat})$ scenario, the 95% CL reach for $\tan \beta = 10$ extends to $m_A \sim 1$ TeV whilst for $\tan \beta = 40$ the Run 3 exclusion extends to $m_A \sim 2$ TeV. Thus, comparing the Run 2 139 fb^{-1} exclusion to that expected from LHC Run 3, we find an extra gain in exclusion of m_A of $\sim 0.1\text{--}0.2$ TeV. The presence of (natural) SUSY decay modes tends to reduce the LHC exclusion by ~ 0.2 TeV compared to the hMSSM.

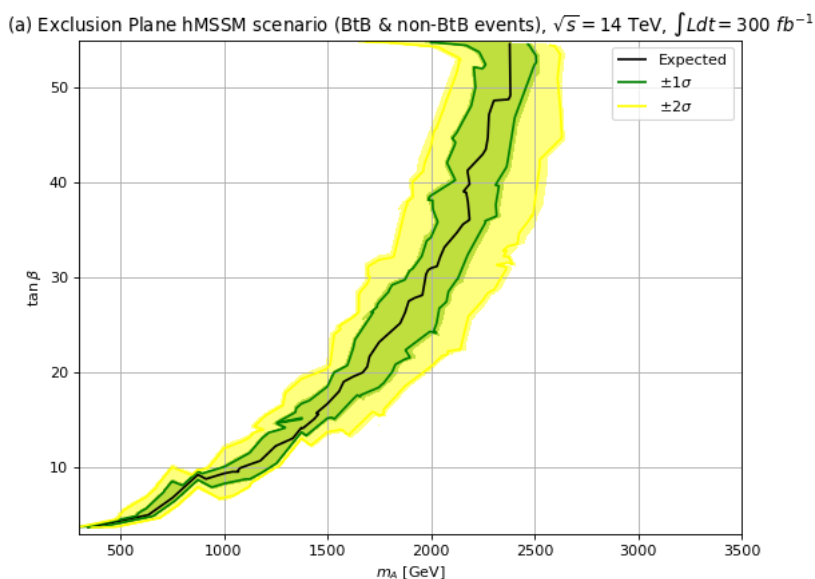


Figure 12. Cont.

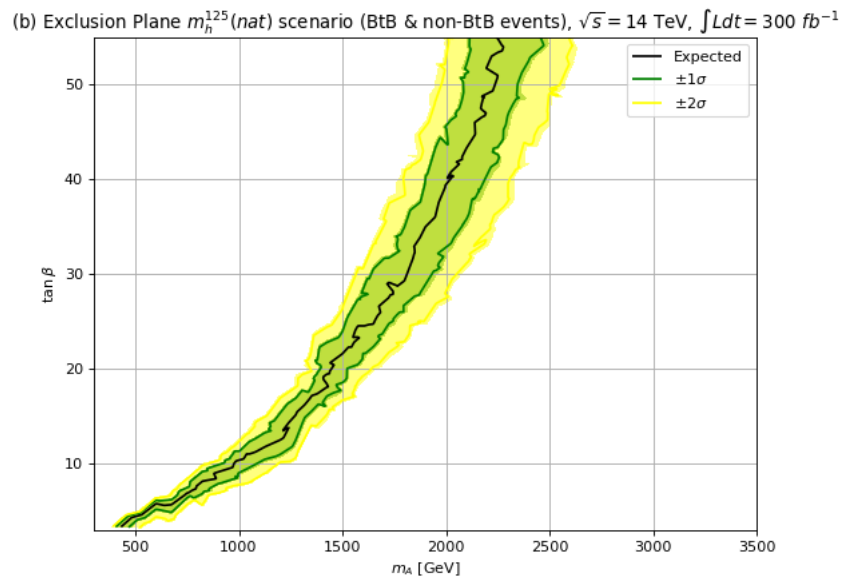


Figure 12. The 95% CL upper limits with $\sqrt{s} = 14$ TeV and 300 fb^{-1} for $H, A \rightarrow \tau\bar{\tau}$ in (a) the hMSSM and (b) the $m_h^{125}(\text{nat})$ scenario.

In Figure 13, we plot our projected exclusion limits of HL-LHC for $H, A \rightarrow \tau\bar{\tau}$ at $\sqrt{s} = 14$ TeV with 3000 fb^{-1} . From frame *a*) in the hMSSM case, we find a HL-LHC 95% CL exclusion out to $m_A \sim 1.5$ TeV for $\tan\beta = 10$ and out to $m_A \sim 2.8$ TeV for $\tan\beta = 40$. If instead we invoke the $m_h^{125}(\text{nat})$ SUSY scenario, then the corresponding HL-LHC exclusion drops to $m_A \sim 1.3$ TeV for $\tan\beta = 10$ and to $m_A \sim 2.6$ TeV for $\tan\beta = 40$, i.e., a drop in reach of about 0.2 TeV in moving from the hMSSM to the $m_h^{125}(\text{nat})$ scenario.

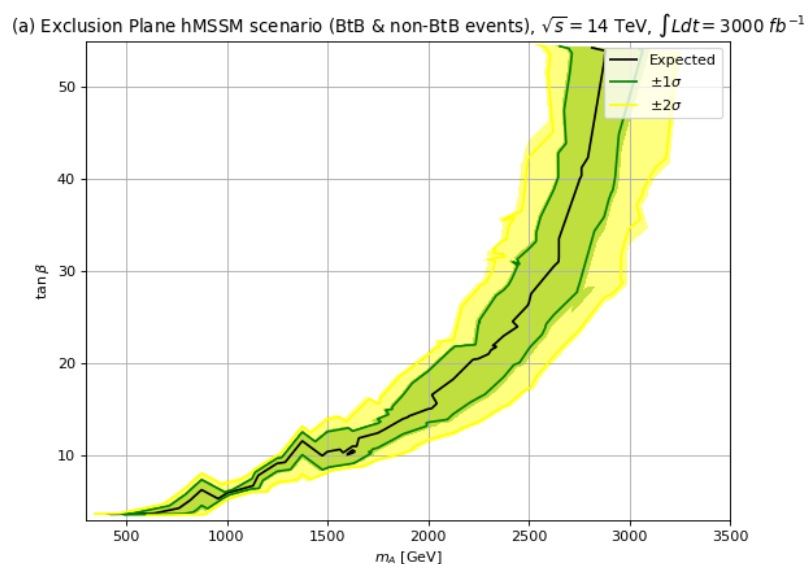


Figure 13. Cont.

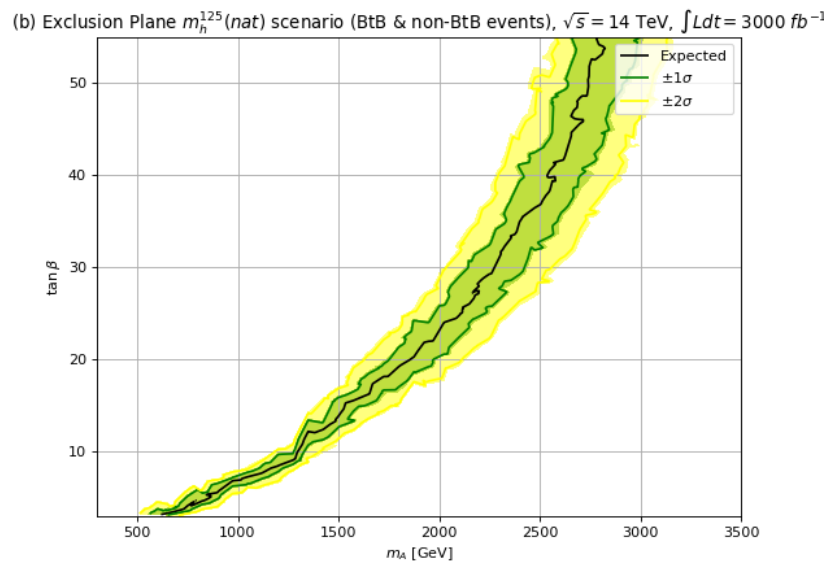


Figure 13. The 95% CL upper limits with $\sqrt{s} = 14 \text{ TeV}$ and 3000 fb^{-1} for $H, A \rightarrow \tau\bar{\tau}$ in (a) the hMSSM and (b) the $m_h^{125}(\text{nat})$ scenario.

6.2. Discovery Plane

To compare with the ATLAS reach in the discovery plane obtained in their Run 2 search with 139 fb^{-1} , we show our corresponding results in Figure 14. For this plot, we use only the BtB signal in the hMSSM where m_h is set to 125 GeV, which should compare well with the m_h^{125} scenario used by ATLAS which contains sparticles at or around 2 TeV, i.e., presumably SUSY decay modes are closed for most m_A values shown in the plot. From Figure 14, we see our expected 5σ reach extends to $m_A \sim 0.75 \text{ TeV}$ for $\tan\beta = 10$ which compares favorably with ATLAS. For $\tan\beta = 40$, we obtain a 5σ reach of $m_A \sim 1.7 \text{ TeV}$, which is somewhat better than the ATLAS expected reach of $m_A \sim 1.6 \text{ TeV}$.

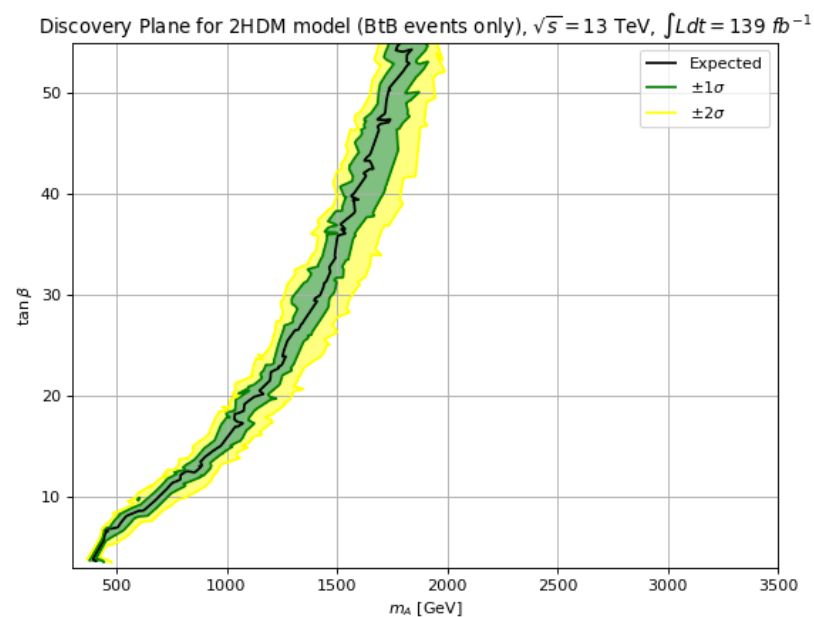


Figure 14. The discovery sensitivity at 5σ level with $\sqrt{s} = 13 \text{ TeV}$ and 139 fb^{-1} for $H, A \rightarrow \tau\bar{\tau}$ using BtB signal only in the hMSSM.

In Figure 15, we plot in frame (a) our expected Run 2 discovery reach assuming 139 fb^{-1} using the combined BtB and acollinear signal channels in the hMSSM. The 5σ discovery reach for $\tan \beta = 10$ extends to $m_A = 0.7 \text{ TeV}$ and for $\tan \beta = 40$ to $m_A = 1.7 \text{ TeV}$. For frame (b), for the $m_h^{125}(\text{nat})$ scenario, then the corresponding 139 fb^{-1} 5σ discovery reach extends to $m_A \sim 0.7 \text{ TeV}$ for $\tan \beta = 10$ and to $m_A \sim 1.6 \text{ TeV}$ for $\tan \beta = 40$.

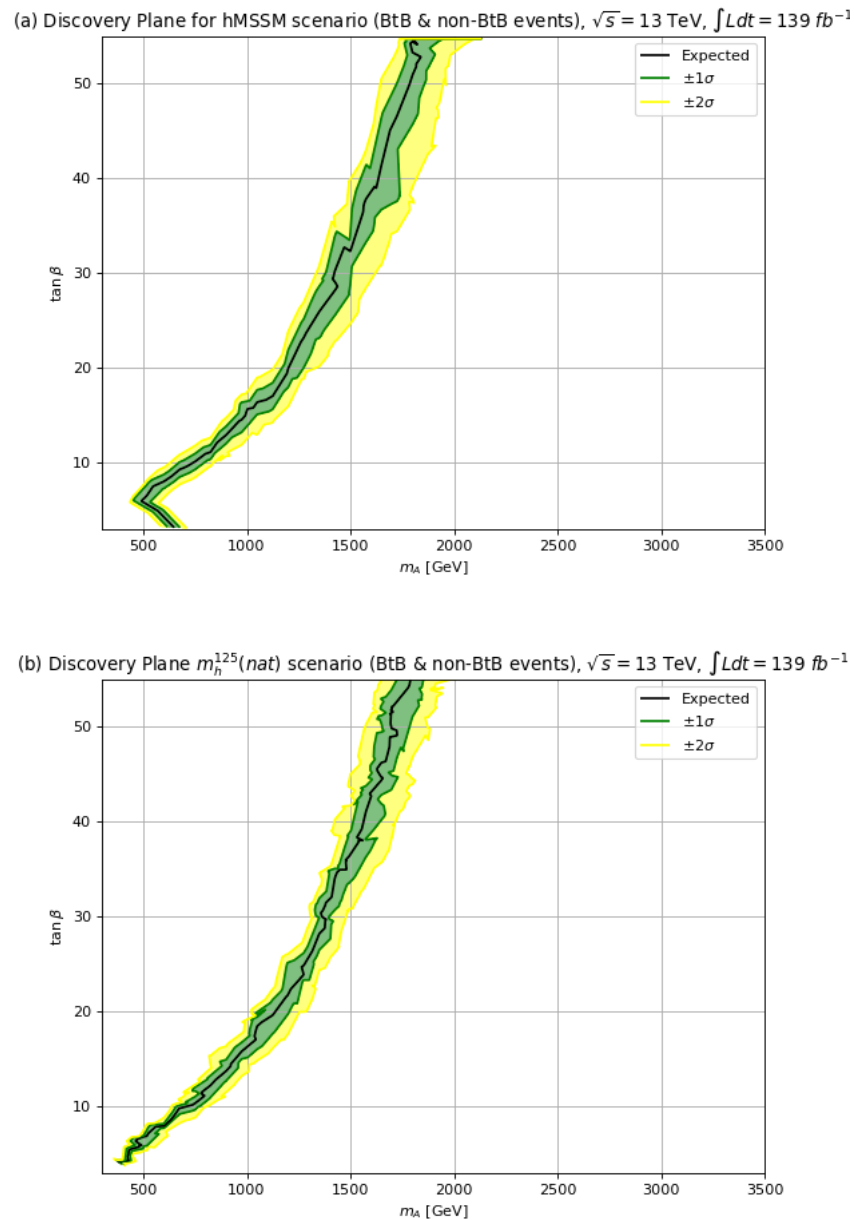


Figure 15. The discovery sensitivity with $\sqrt{s} = 13 \text{ TeV}$ and 139 fb^{-1} for $H, A \rightarrow \tau\bar{\tau}$ in the (a) the hMSSM and (b) the $m_h^{125}(\text{nat})$ scenario.

In Figure 16, we present our future 5σ discovery sensitivity reach, this time for LHC collisions at $\sqrt{s} = 14 \text{ TeV}$ with 300 fb^{-1} of integrated luminosity, as would be expected from LHC Run 3. Here, we use both the BtB and acollinear signals. For Run 3, we see in frame a) for the hMSSM the $\tan \beta = 10$ discovery reach extends out to $m_A \sim 0.8 \text{ TeV}$ while the $\tan \beta = 40$ reach extends to $m_A \sim 1.8 \text{ TeV}$. For the frame b) case with the $m_h^{125}(\text{nat})$ scenario, the discovery sensitivity reach for $\tan \beta = 10$ extends to $m_A \sim 0.75 \text{ TeV}$ whilst for $\tan \beta = 40$ the Run 3 reach extends to $m_A \sim 1.75 \text{ TeV}$. Thus, comparing the Run 2

139 fb^{-1} reach to that expected from LHC Run 3, we find an extra gain in reach of m_A of $\sim 0.1\text{--}0.2 \text{ TeV}$. The presence of (natural) SUSY decay modes tends to reduce the LHC reach by $\sim 0.1 \text{ TeV}$ compared to the hMSSM.

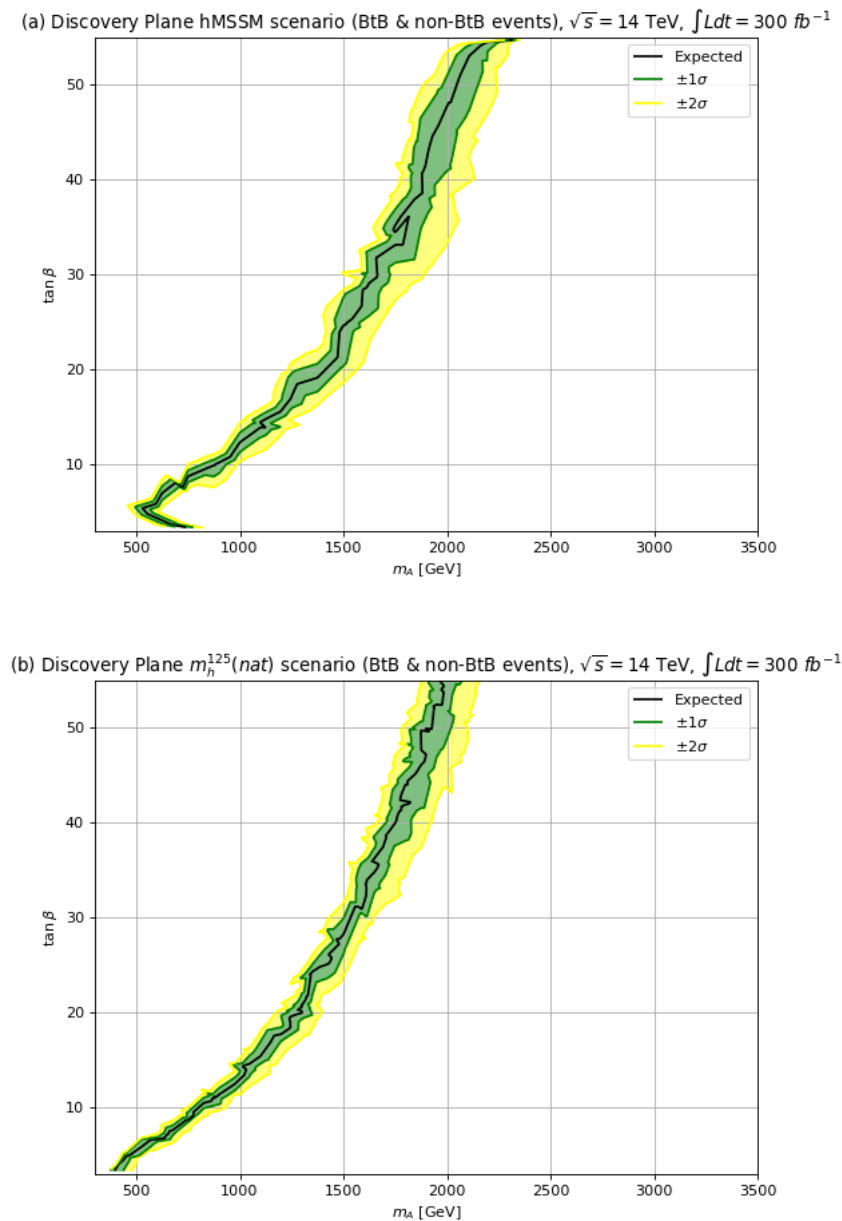


Figure 16. The discovery sensitivity with $\sqrt{s} = 14 \text{ TeV}$ and 300 fb^{-1} for $H, A \rightarrow \tau\bar{\tau}$ in (a) the hMSSM and (b) the $m_h^{125}(\text{nat})$ scenario.

In Figure 17, we plot our discovery reach of HL-LHC for $H, A \rightarrow \tau\bar{\tau}$ at $\sqrt{s} = 14 \text{ TeV}$ with 3000 fb^{-1} . From frame (a) in the hMSSM case, we find a HL-LHC discovery sensitivity reach out to $m_A \sim 1.25 \text{ TeV}$ for $\tan\beta = 10$ and out to $m_A \sim 2.45 \text{ TeV}$ for $\tan\beta = 40$. If instead we invoke the $m_h^{125}(\text{nat})$ SUSY scenario, then the corresponding HL-LHC reaches drop to $m_A \sim 1.15 \text{ TeV}$ for $\tan\beta = 10$ and to $m_A \sim 2.25 \text{ TeV}$ for $\tan\beta = 40$, i.e., a drop in reach of about 0.2 TeV in moving from the hMSSM to the $m_h^{125}(\text{nat})$ scenario.

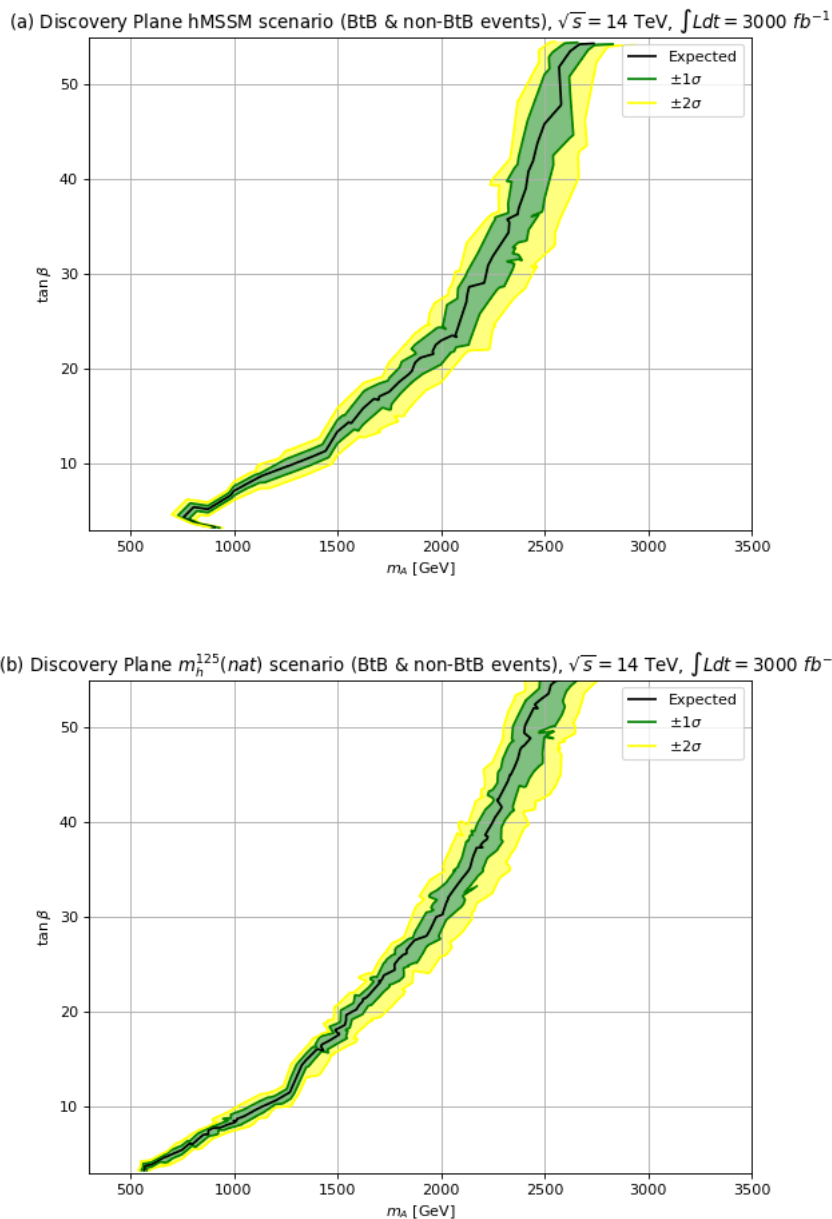


Figure 17. The discovery sensitivity with $\sqrt{s} = 14$ TeV and 3000 fb^{-1} for $H, A \rightarrow \tau\bar{\tau}$ in (a) the hMSSM and (b) the $m_h^{125}(\text{nat})$ scenario.

6.3. Comparing Reach Results to Expectations from the String Landscape

It is instructive to compare the various LHC upgrade reach in m_A to recent theoretical predictions for SUSY Higgs bosons from the string landscape picture [15], which also offers a solution to the cosmological constant problem. In a statistical scan of pocket universes within the greater multiverse as expected from the string landscape, one expects a power-law draw to large soft terms [62], including $m_{H_d}^2$ which tends to set the mass scale for $m_{A,H}$. However, the draw to large soft terms is tempered by the requirement that contributions to the weak scale should not lie outside the Agrawal-Barr-Donoghue-Seckel (ABDS) anthropic window [63] lest the weak scale become too big and complex nuclei and hence atoms as we know them do not form (atomic principle). In such a setting, the expected statistical predictions in the m_A vs. $\tan\beta$ plane were plotted in Figure 9 of Ref. [64]. In that Figure, the string landscape with an $n = 1$ power-law draw to large soft terms typically has m_A extending from 1 to 8 TeV with $\tan\beta \sim 10\text{--}20$. By comparing our LHC reach plots

from either exclusion plane or discovery plane with the string landscape expectation, we see that even HL-LHC will only probe a small portion of the theory-expected region of parameter space.

7. Conclusions

In this paper, we have re-examined the current LHC and LHC-upgrades reach for SUSY Higgs bosons in a natural SUSY model with $m_h \simeq 125$ GeV. This led us to propose the $m_h^{125}(\text{nat})$ scenario where a 100 GeV weak scale emerges because all contributions to the weak scale are comparable to or less than the measured weak scale, in accord with practical naturalness. This scenario is a more plausible SUSY benchmark than many others proposed in the literature in that it requires no implausible finetunings of parameters in order to gain a value for the weak scale in accord with its measured value. The price of this natural SUSY scenario is that for $m_A \gtrsim 1\text{--}2$ TeV, as is being presently explored at LHC, the H, A decay modes to gaugino+higgsino are frequently open and can even dominate the heavy Higgs branching ratios, thus diluting the value of the $H, A \rightarrow \tau\bar{\tau}$ branching fraction as expected in the hMSSM, or other unnatural SUSY models with a heavy spectrum of SUSY particles.

We also revisited the $H, A \rightarrow \tau\bar{\tau}$ discovery channels. Along with the channel used by ATLAS and CMS of BtB ditaus, we advocated for inclusion of acollinear ditaus where the ditau invariant mass can be reconstructed under the assumption that the daughter neutrinos from τ lepton decay are collinear with the parent τ direction. This additional signal channel can substantially increase the signal compared to using only the BtB ditau channel.

Using the combined BtB and acollinear ditau signals along with the $m_h^{125}(\text{nat})$ scenario (and the hMSSM for comparison), we evaluated the present LHC and future LHC upgrades exclusion limits and 5σ discovery reach for $H, A \rightarrow \tau\bar{\tau}$ in the m_A vs. $\tan\beta$ plane. For $\tan\beta = 10$, the reach for m_A in the $m_h^{125}(\text{nat})$ scenario for Run 2 (Run 3) ((HL-LHC)) extends to $m_A \sim 1$ TeV (1.1 TeV) ((1.4 TeV)). This will probe some additional chunk of parameter space, although string landscape predictions allow m_A values up to ~ 8 TeV, so much higher energy hadron colliders will be needed for a complete coverage of heavy Higgs boson parameter space.

Author Contributions: Conceptualization, H.B., V.B., X.T. and K.Z.; methodology, K.Z.; software, K.Z.; validation, H.B., V.B., X.T. and K.Z.; formal analysis, H.B., V.B., X.T. and K.Z.; investigation, H.B. and K.Z.; resources, V.B.; data curation, n/a; writing—original draft preparation, H.B.; writing—review and editing, H.B., V.B., X.T. and K.Z.; visualization, n/a; supervision, H.B., V.B., X.T. and K.Z.; project administration, H.B., V.B., X.T. and K.Z.; funding acquisition, H.B. and V.B. All authors have read and agreed to the published version of the manuscript.

Funding: This research was funded by U.S. Department of Energy, Office of Science, Office of high Energy Physics grant number DE-SC-0009956 and DE-SC-0017647.

Institutional Review Board Statement: Not applicable.

Informed Consent Statement: Not applicable.

Acknowledgments: This material is based upon work supported by the U.S. Department of Energy, Office of Science, Office of High Energy Physics under Award Number DE-SC-0009956 and DE-SC-0017647.

Conflicts of Interest: The authors declare no conflict of interest.

References

1. Carena, M.; Heinemeyer, S.; Stål, O.; Wagner, C.E.M.; Weiglein, G. MSSM Higgs Boson Searches at the LHC: Benchmark Scenarios after the Discovery of a Higgs-like Particle. *Eur. Phys. J. C* **2013**, *73*, 2552. [[CrossRef](#)]
2. Djouadi, A.; Maiani, L.; Moreau, G.; Polosa, A.; Quevillon, J.; Riquer, V. The post-Higgs MSSM scenario: Habemus MSSM? *Eur. Phys. J. C* **2013**, *73*, 2650. [[CrossRef](#)]
3. Djouadi, A.; Maiani, L.; Polosa, A.; Quevillon, J.; Riquer, V. Fully covering the MSSM Higgs sector at the LHC. *JHEP* **2015**, *6*, 168. [[CrossRef](#)]
4. Bagnaschi, E.; Bahl, H.; Fuchs, E.; Hahn, T.; BHeinemeyer, S.; Liebler, S.; Patel, S.; Slavich, P.; BStefaniak, T.; Wagner, C.E.; et al. MSSM Higgs Boson Searches at the LHC: Benchmark Scenarios for Run 2 and Beyond. *Eur. Phys. J. C* **2019**, *79*, 617. [[CrossRef](#)]

5. Bahl, H.; Bechtler, P.; Heinemeyer, S.; Liebler, S.; Stefaniak, T.; Weiglein, G. HL-LHC and ILC sensitivities in the hunt for heavy Higgs bosons. *Eur. Phys. J. C* **2020**, *80*, 916. [[CrossRef](#)]
6. Baer, H.; Barger, V.; Martinez, D.; Salam, S. Fine-tuned vs. natural supersymmetry: What does the string landscape predict? *J. High Energy Phys.* **2022**, *2022*, 125. [[CrossRef](#)]
7. Baer, H.; Barger, V.; Savoy, M. Upper bounds on sparticle masses from naturalness or how to disprove weak scale supersymmetry. *Phys. Rev. D* **2016**, *93*, 035016. [[CrossRef](#)]
8. Baer, H.; Tata, X. *Weak Scale Supersymmetry: From Superfields to Scattering Events*; Cambridge University Press: Cambridge, MA, USA, 2006.
9. Baer, H.; Barger, V.; Huang, P.; Mickelson, D.; Mustafayev, A.; Tata, X. Radiative natural supersymmetry: Reconciling electroweak fine-tuning and the Higgs boson mass. *Phys. Rev. D* **2013**, *87*, 115028. [[CrossRef](#)]
10. Baer, H.; Barger, V.; Martinez, D. Comparison of SUSY spectra generators for natural SUSY and string landscape predictions. *Eur. Phys. J. C* **2022**, *82*, 172. [[CrossRef](#)]
11. Dedes, A.; Slavich, P. Two loop corrections to radiative electroweak symmetry breaking in the MSSM. *Nucl. Phys. B* **2003**, *657*, 333–354. [[CrossRef](#)]
12. Baer, H.; Barger, V.; Huang, P.; Mustafayev, A.; Tata, X. Radiative natural SUSY with a 125 GeV Higgs boson. *Phys. Rev. Lett.* **2012**, *109*, 161802. [[CrossRef](#)]
13. Bae, K.J.; Baer, H.; Barger, V.; Sengupta, D. Revisiting the SUSY μ problem and its solutions in the LHC era. *Phys. Rev. D* **2019**, *99*, 115027. [[CrossRef](#)]
14. Bae, K.J.; Baer, H.; Barger, V.; Mickelson, D.; Savoy, M. Implications of naturalness for the heavy Higgs bosons of supersymmetry. *Phys. Rev. D* **2014**, *90*, 075010. [[CrossRef](#)]
15. Baer, H.; Barger, V.; Salam, S.; Sengupta, D.; Sinha, K. Status of weak scale supersymmetry after LHC Run 2 and ton-scale noble liquid WIMP searches. *Eur. Phys. J. ST* **2020**, *229*, 3085–3141. [[CrossRef](#)]
16. Slavich, P.; Heinemeyer, S.; Bagnaschi, E.; Bahl, H.; Goodsell, M.; Haber, H.E.; Hahn, T.; Harlander, R.; Hollik, W.; Lee, G.; et al. Higgs-mass predictions in the MSSM and beyond. *Eur. Phys. J. C* **2021**, *81*, 450. [[CrossRef](#)]
17. ATLAS Collaboration; Aaboud, M.; Aad, G.; Abbott, B.; Abdallah, J.; Abdinov, O.; Abeloos, B.; Aben, R.; AbouZeid, O.S. Search for squarks and gluinos in final states with jets and missing transverse momentum using 139 fb^{-1} of $\sqrt{s} = 13 \text{ TeV}$ pp collision data with the ATLAS detector. *JHEP* **2021**, *2*, 143. [[CrossRef](#)]
18. The CMS Collaboration; Sirunyan, A.M.; Tumasyan, A.; Adam, W.; Ambrogio, F.; Bergauer, T.; Brandstetter, J.; Dragicevic, M.; Erö, J.; Valle, A.E.D.; et al. Search for supersymmetry in proton-proton collisions at 13 TeV in final states with jets and missing transverse momentum. *JHEP* **2019**, *10*, 244. [[CrossRef](#)]
19. Branco, G.C.; Ferreira, P.M.; Lavoura, L.; Rebelo, M.N.; Sher, M.; Silva, J.P. Theory and phenomenology of two-Higgs-doublet models. *Phys. Rep.* **2012**, *516*, 1–102. [[CrossRef](#)]
20. Gunion, J.F.; Haber, H.E. The CP conserving two Higgs doublet model: The Approach to the decoupling limit. *Phys. Rev. D* **2003**, *67*, 075019. [[CrossRef](#)]
21. Carena, M.; Low, I.; Shah, N.R.; Wagner, C.E.M. Impersonating the Standard Model Higgs Boson: Alignment without Decoupling. *JHEP* **2014**, *4*, 15. [[CrossRef](#)]
22. Arcadi, G.; Djouadi, A.; He, H.J.; Kneur, J.L.; Xiao, R.Q. The hMSSM with a Light Gaugino/Higgsino Sector: Implications for Collider and Astroparticle Physics. *arXiv* **2022**, arXiv:2206.11881.
23. Aad, G.; et al. Search for heavy Higgs bosons decaying into two tau leptons with the ATLAS detector using pp collisions at $\sqrt{s} = 13 \text{ TeV}$. *Phys. Rev. Lett.* **2020**, *125*, 051801. [[CrossRef](#)]
24. Barger, V.D.; Martin, A.D.; Phillips, R.J.N. Sharpening Up the $W \rightarrow T \bar{b}$ Signal. *Phys. Lett. B* **1985**, *151*, 463–468. [[CrossRef](#)]
25. Sirunyan, A.M.; et al. Search for additional neutral MSSM Higgs bosons in the $\tau\tau$ final state in proton-proton collisions at $\sqrt{s} = 13 \text{ TeV}$. *JHEP* **2018**, *9*, 7. [[CrossRef](#)]
26. Cepeda, M.; Gori, S.; Ilten, P.; Kado, M.; Riva, F. Report from Working Group 2: Higgs Physics at the HL-LHC and HE-LHC. *CERN Yellow Rep. Monogr.* **2019**, *7*, 221–584. [[CrossRef](#)]
27. Bahl, H.; Liebler, S.; Stefaniak, T. MSSM Higgs benchmark scenarios for Run 2 and beyond: The low $\tan \beta$ region. *Eur. Phys. J. C* **2019**, *79*, 279. [[CrossRef](#)]
28. Baer, H.; Barger, V.; Sengupta, D. Anomaly mediated SUSY breaking model retrofitted for naturalness. *Phys. Rev. D* **2018**, *98*, 015039. [[CrossRef](#)]
29. Baer, H.; Barger, V.; Serce, H.; Tata, X. Natural generalized mirage mediation. *Phys. Rev. D* **2016**, *94*, 115017. [[CrossRef](#)]
30. Choi, K.; Falkowski, A.; Nilles, H.P.; Olechowski, M. Soft supersymmetry breaking in KKLT flux compactification. *Nucl. Phys. B* **2005**, *718*, 113–133. [[CrossRef](#)]
31. Kachru, S.; Kallosh, R.; Linde, A.D.; Trivedi, S.P. De Sitter vacua in string theory. *Phys. Rev. D* **2003**, *68*, 046005. [[CrossRef](#)]
32. Broeckel, I.; Cicoli, M.; Maharana, A.; Singh, K.; Sinha, K. Moduli Stabilisation and the Statistics of SUSY Breaking in the Landscape. *JHEP* **2020**, *10*, 15. [[CrossRef](#)]
33. Ellis, J.R.; Olive, K.A.; Santoso, Y. The MSSM parameter space with nonuniversal Higgs masses. *Phys. Lett. B* **2002**, *539*, 107–118. [[CrossRef](#)]
34. Baer, H.; Mustafayev, A.; Profumo, S.; Belyaev, A.; Tata, X. Direct, indirect and collider detection of neutralino dark matter in SUSY models with non-universal Higgs masses. *JHEP* **2005**, *7*, 65. [[CrossRef](#)]

35. Baer, H.; Barger, V.; Sengupta, D. Landscape solution to the SUSY flavor and CP problems. *Phys. Rev. Res.* **2019**, *1*, 033179. [[CrossRef](#)]
36. Paige, F.E.; Protopopescu, S.D.; Baer, H.; Tata, X. ISAJET 7.69: A Monte Carlo event generator for pp, anti-p p, and e+e- reactions. *arXiv* **2003**, arXiv:hep-ph/0312045.
37. Baer, H.; Chen, C.H.; Munroe, R.B.; Paige, F.E.; Tata, X. Multichannel search for minimal supergravity at $p\bar{p}$ and e^+e^- colliders. *Phys. Rev. D* **1995**, *51*, 1046–1050. [[CrossRef](#)]
38. Aalbers, J.; Akerib, D.S.; Akerlof, C.W.; Al Musalhi, A.K.; Alder, F.; Alqahtani, A.; Alsum, S.K.; Amarasinghe, C.S.; Ames, A.; Anderson, T.J.; et al. First Dark Matter Search Results from the LUX-ZEPLIN (LZ) Experiment. *arXiv* **2022**, arXiv:2207.03764.
39. Aprile, E.; Aalbers, J.; AAgosti, F.; Alfonsi, M.; AAlthueser, L.; Amaro, F.D.; Anthony, M.; Arneodo, F.; Baudis, L.; Bauermeister, B.; et al. Dark Matter Search Results from a One Ton-Year Exposure of XENON1T. *Phys. Rev. Lett.* **2018**, *121*, 111302. [[CrossRef](#)] [[PubMed](#)]
40. Cui, X.; AAbdukeri, A.; Chen, W.; Chen, X.; Chen, Y.; Dong, B.; AFang, D.; Au, C.; Giboni, K.; Giuliani, F.; et al. Dark Matter Results From 54-Ton-Day Exposure of PandaX-II Experiment. *Phys. Rev. Lett.* **2017**, *119*, 181302. [[CrossRef](#)]
41. Baer, H.; Barger, V.; Serce, H. SUSY under siege from direct and indirect WIMP detection experiments. *Phys. Rev. D* **2016**, *94*, 115019. [[CrossRef](#)]
42. Bae, K.J.; Baer, H.; Lessa, A.; Serce, H. Coupled Boltzmann computation of mixed axion neutralino dark matter in the SUSY DFSZ axion model. *JCAP* **2014**, *10*, 82. [[CrossRef](#)]
43. Bae, K.J.; Baer, H.; Barger, V.; Deal, R.W. The cosmological moduli problem and naturalness. *JHEP* **2022**, *2*, 138. [[CrossRef](#)]
44. Gelmini, G.B.; Gondolo, P. Neutralino with the right cold dark matter abundance in (almost) any supersymmetric model. *Phys. Rev. D* **2006**, *74*, 023510. [[CrossRef](#)]
45. Bisset, M.A. Detection of Higgs Bosons of the Minimal Supersymmetric Standard Model at Hadron Supercolliders. Ph.D. Thesis, UMI-95-32579, 1995.
46. Pierce, D.M.; Bagger, J.A.; Matchev, K.T.; Zhang, R.J. Precision corrections in the minimal supersymmetric standard model. *Nucl. Phys. B* **1997**, *491*, 3–67. [[CrossRef](#)]
47. Carena, M.; Haber, H.E. Higgs Boson Theory and Phenomenology. *Prog. Part. Nucl. Phys.* **2003**, *50*, 63–152. [[CrossRef](#)]
48. Bahl, H.; Hahn, T.; Heinemeyer, S.; Hollik, W.; Paßehr, S.; Rzehak, H.; Weiglein, G. Precision calculations in the MSSM Higgs-boson sector with FeynHiggs 2.14. *Comput. Phys. Commun.* **2020**, *249*, 107099. [[CrossRef](#)]
49. Harlander, R.V.; Liebler, S.; Mantler, H. SusHi: A program for the calculation of Higgs production in gluon fusion and bottom-quark annihilation in the Standard Model and the MSSM. *Comput. Phys. Commun.* **2013**, *184*, 1605–1617. [[CrossRef](#)]
50. Kunszt, Z.; Zwirner, F. Testing the Higgs sector of the minimal supersymmetric standard model at large hadron colliders. *Nucl. Phys. B* **1992**, *385*, 3–75. [[CrossRef](#)]
51. Baer, H.; Dicus, D.; Drees, M.; Tata, X. Higgs Boson Signals in Superstring Inspired Models at Hadron Supercolliders. *Phys. Rev. D* **1987**, *36*, 1363. [[CrossRef](#)]
52. Gunion, J.F.; Haber, H.E.; Drees, M.; Karatas, D.; Tata, X.; Godbole, R.; Tracas, N. Decays of Higgs Bosons to Neutralinos and Charginos in the Minimal Supersymmetric Model: Calculation and Phenomenology. *Int. J. Mod. Phys. A* **1987**, *2*, 1035. [[CrossRef](#)]
53. Gunion, J.F.; Haber, H.E. Higgs Bosons in Supersymmetric Models. 3. Decays Into Neutralinos and Charginos. *Nucl. Phys. B* **1988**, *307*, 445. [Erratum: *Nucl.Phys.B* 402, 569 (1993)]. [[CrossRef](#)]
54. Eriksson, D.; Rathsman, J.; Stal, O. 2HDMC: Two-Higgs-Doublet Model Calculator Physics and Manual. *Comput. Phys. Commun.* **2010**, *181*, 189–205. [[CrossRef](#)]
55. Bae, K.J.; Baer, H.; Nagata, N.; Serce, H. Prospects for Higgs coupling measurements in SUSY with radiatively-driven naturalness. *Phys. Rev. D* **2015**, *92*, 035006. [[CrossRef](#)]
56. Baer, H.; Barger, V.; Jain, R.; Kao, C.; Sengupta, D.; Tata, X. Detecting heavy Higgs bosons from natural SUSY at a 100 TeV hadron collider. *Phys. Rev. D* **2022**, *105*, 095039. [[CrossRef](#)]
57. Baer, H.; Kraml, S.; Kulkarni, S. Yukawa-unified natural supersymmetry. *JHEP* **2012**, *12*, 66. [[CrossRef](#)]
58. Sjostrand, T.; Mrenna, S.; Skands, P.Z. A Brief Introduction to PYTHIA 8.1. *Comput. Phys. Commun.* **2008**, *178*, 852–867. [[CrossRef](#)]
59. de Favereau, J.; Delaere, C.; Demin, P.; Giammanco, A.; Lemaître, V.; Mertens, A.; Selvaggi, M. DELPHES 3, A modular framework for fast simulation of a generic collider experiment. *JHEP* **2014**, *2*, 57. [[CrossRef](#)]
60. Read, A.L. Presentation of search results: The CL_s technique. *J. Phys. G* **2002**, *28*, 2693. [[CrossRef](#)]
61. Cowan, G.; Cranmer, K.; Gross, E.; Vitells, O. Asymptotic formulae for likelihood-based tests of new physics. *Eur.Phys. J. C* **2011**, *71*, 1554. [[CrossRef](#)]
62. Douglas, M.R. Statistical analysis of the supersymmetry breaking scale. *arXiv* **2004**, arXiv:hep-th/0405279.
63. Agrawal, V.; Barr, S.M.; Donoghue, J.F.; Seckel, D. Anthropic considerations in multiple domain theories and the scale of electroweak symmetry breaking. *Phys. Rev. Lett.* **1998**, *80*, 1822–1825. [[CrossRef](#)]
64. Baer, H.; Barger, V.; Salam, S.; Serce, H.; Sinha, K. LHC SUSY and WIMP dark matter searches confront the string theory landscape. *JHEP* **2019**, *4*, 43. [[CrossRef](#)]